Effector-mediated subversion of proteasome activator (PA)28αβ enhances host defense against *Legionella pneumophila* under inflammatory and oxidative stress conditions

Tshegofatso Ngwaga[1], Deepika Chauhan[1,#,¶], Abigail G. Salberg[1,¶], and Stephanie R. Shames[1,2]*

[1]Division of Biology, Kansas State University, Manhattan, Kansas, USA

[2]Department of Microbiology & Molecular Genetics, Michigan State University, East Lansing, Michigan, USA

[#]Current address: Department of Veterinary Pathobiology, University of Missouri, Columbia, Missouri, USA

*Corresponding author:

Email: shames@msu.edu

Phone: (517) 884-5364

Short title: PA28αβ- and effector-mediated host defense

Keywords: PA28, proteasome, phagolysosomal fusion, cytokines, cell-autonomous immunity, *Legionella pneumophila*, LegC4, proteostasis, oxidative stress

¶these authors contributed equally to this work

Abstract

Legionella pneumophila is a natural pathogen of amoebae that causes Legionnaires' Disease in immunocompromised individuals via replication within macrophages. *L. pneumophila* virulence and intracellular replication hinges on hundreds of Dot/Icm-translocated effector proteins, which are essential for biogenesis of the replication permissive *Legionella*-containing vacuole (LCV). However, effector activity can also enhance mammalian host defense via effector-triggered immunity. The *L. pneumophila* effector LegC4 is important for virulence in amoebae but enhances host defense against *L. pneumophila* in the mouse lung and, uniquely, within macrophages activated with either tumor necrosis factor (TNF) or interferon (IFN)-γ. The mechanism by which LegC4 potentiates cytokine-mediated host defense in macrophages is unknown. Here, we found that LegC4 enhances cytokine-mediated phagolysosomal fusion with *Legionella*-containing vacuole (LCV) and binds host proteasome activator (PA)28α, which forms a heterooligomer with PA28β to facilitate ubiquitin-independent proteasomal degradation of oxidant-damaged (carbonylated) proteins. We found that oxidative stress was sustained in the presence of LegC4 and that the LegC4 restriction phenotype was relieved in PA28$\alpha\beta$-deficient macrophages and in the lungs of mice *in vivo*. Our data also show that oxidative stress is sufficient for LegC4-mediated restriction in macrophages producing PA28$\alpha\beta$. PA28$\alpha\beta$ has been traditionally associated with antigen presentation; however, our data support a novel mechanism whereby effector-mediated subversion of PA28$\alpha\beta$ enhances cell-autonomous host defense against *L. pneumophila* under inflammatory and oxidative stress conditions. This work provides a solid foundation to evaluate induced proteasome regulators as mediators of innate immunity.

Author Summary

Pro-inflammatory cytokines induce antimicrobial host defense pathways within macrophages to control intracellular pathogens. We discovered that the *Legionella pneumophila* effector protein LegC4 potentiates pathogen clearance within cytokine-activated macrophages. Here, we show a central role for host proteasome activator (PA)28αβ in LegC4 restriction. PA28αβ is upregulated by cytokine signaling and under oxidative stress conditions to facilitate proteasomal degradation of oxidant-damaged proteins. We found that LegC4 binds PA28αβ and that LegC4 restriction was lost in PA28αβ-deficient (*Psme1/2*$^{-/-}$) macrophages and a mouse model of Legionnaires' Disease *in vivo*. Furthermore, oxidative stress was sustained in the presence of LegC4 and was sufficient for LegC4 restriction in PA28αβ-producing cells macrophages. Finally, we found that *L. pneumophila* replication was attenuated within PA28αβ-deficient macrophages irrespective of LegC4. These findings support a model whereby subversion of host proteostasis machinery triggers cell-autonomous host defense within macrophages under inflammatory and oxidative stress conditions.

64 **Introduction**

65 Many intracellular bacterial pathogens cause disease by replicating within host macrophages [1].
66 However, macrophages activated by T_H1 proinflammatory cytokines, such as tumor necrosis fac-
67 tor (TNF) and interferon (IFN)-γ, are potently and broadly microbicidal. However, activated mac-
68 rophages and inflamed tissues are in a state of altered protein homeostasis (proteostasis), owing
69 in part to robust production of reactive oxygen species (ROS), which cause collateral damage to
70 cellular proteins. To cope with this oxidative stress, cytokine signaling and ROS upregulate pro-
71 teasome activator (PA)28$\alpha\beta$, which engages proteolytic 20S proteasome core particles (CPs) to
72 facilitate rapid ubiquitin-independent degradation of oxidant-damaged proteins [2]. Impaired pro-
73 teasome activity and proteotoxic stress trigger compensatory upregulation of lysosomal degrada-
74 tion pathways, which are central to cell-autonomous immunity within activated macrophages [3].
75 PA28$\alpha\beta$ has been traditionally associated with antigen presentation and adaptive immunity [4,5];
76 however, a role for PA28$\alpha\beta$ in cell-autonomous antimicrobial innate host defense has not been
77 established.

78

79 *Legionella pneumophila* is a natural pathogen of amoebae and accidental human pathogen that
80 causes Legionnaires' Disease pneumonia in immunocompromised individuals that results from
81 bacterial replication within alveolar macrophages [6]. *L. pneumophila* replication within macro-
82 phages is a direct consequence of extensive co-evolution with natural host amoebae [7–9]; how-
83 ever, *L. pneumophila* rarely transmits person-to-person and is rapidly cleared by acute pathogen-
84 centric innate immune responses in healthy hosts [10–12]. To establish its intracellular niche, the
85 *Legionella*-containing vacuole (LCV), *L. pneumophila* translocates hundreds of virulence factors,
86 called effector proteins, into infected host cells by a Dot/Icm type IV secretion system (T4SS)
87 [6,13,14]. Effectors are essential for virulence, but detection of their activity within host cells can
88 induce pro-inflammatory cytokine production via effector-triggered immunity (ETI) [10,15–17].

89 Pro-inflammatory cytokines activate and potentiate the antimicrobial capacity of infected macro-
90 phages and are central to host defense against *L. pneumophila* [18,19]. Thus, *L. pneumophila* is
91 a well-established model pathogen to study mechanisms of pathogen-centric and effector-medi-
92 ated antimicrobial innate immunity.
93
94 We discovered that the *L. pneumophila* effector LegC4 induces a unique mechanism of effector-
95 mediated host defense by potentiating the antimicrobial activity of activated macrophages [20].
96 LegC4 host defense by confers a fitness disadvantage on *L. pneumophila* in a mouse model of
97 Legionnaires' Disease, likely resulting from elevated levels of pro-inflammatory cytokines in the
98 lung since a growth defect is only observed within cultured macrophages when activated with
99 exogenous TNF or IFN-γ [20,21]. The evolutionary basis for retention of LegC4 by *L. pneumophila*
100 stems from its importance for replication within its natural host, *Acanthamoeba castellanii* [21].
101 Thus, LegC4 confers quantifiable opposing phenotypes in natural (protozoa) and 'accidental'
102 (mammalian) hosts, which is noteworthy since the majority of *L. pneumophila* effectors are func-
103 tionally redundant in laboratory models and have no obvious growth phenotypes [21,22]. The
104 specific augmentation of cytokine-mediated restriction by LegC4 represents a potentially novel
105 mechanism of ETI, but how LegC4 functions and potentiates host defense against *L. pneumophila*
106 is unknown.
107
108 Here, we investigated the mechanism of LegC4 restriction within macrophages and found a cen-
109 tral role for PA28$\alpha\beta$ and oxidative stress. We found a central role for PA28$\alpha\beta$, phagolysosomal
110 fusion, and oxidative stress in LegC4-mediated restriction. LegC4 enhanced cytokine-dependent
111 phagolysosomal fusion with LCVs and perpetuated oxidative stress. LegC4 bound host PA28α *in*
112 *vitro* and changed the subcellular localization of PA28α within infected and transfected cells.
113 LegC4 restriction phenotypes were relieved in PA28$\alpha\beta$-deficient (*Psme1/2*$^{-/-}$) BMDMs and the

114 fitness advantage associated with Δ*legC4* mutant bacteria *in vivo* was abolished in *Psme1/2*$^{-/-}$
115 mice. The abundance of oxidant-damaged proteins was increased in the presence of LegC4 and
116 oxidative stress was sufficient to impair replication of LegC4-producing of *L. pneumophila* in
117 BMDMs producing PA28αβ. Importantly, *L. pneumophila* replication was attenuated within
118 *Psme1/2*$^{-/-}$ BMDMs irrespective LegC4, suggesting that impaired PA28αβ activity is sufficient to
119 augment host defense in macrophages and is the mechanism driving LegC4 restriction. Overall,
120 our data support a model whereby PA28α targeting by a translocated effector protein perturbs
121 proteostasis and enhances cell-autonomous restriction of *L. pneumophila* within activated mac-
122 rophages. These data are the first to uncover a role for PA28αβ in innate host defense against
123 an intracellular bacterial pathogen and reveal a novel mechanism by which the antimicrobial ac-
124 tivity of macrophages can be augmented under inflammatory and oxidative stress conditions.
125

126 **Results**

127 **LegC4 confers a fitness disadvantage on *L. pneumophila* in cytokine-activated macro-**
128 **phages and in a mouse model of Legionnaires' Disease.** We previously reported that LegC4
129 confers a fitness disadvantage on *L. pneumophila* in intranasal C57Bl/6 mouse models of Legion-
130 naires' Disease (LD) and within cytokine-activated macrophages [20,21]. C57Bl/6 mice are re-
131 strictive to *L. pneumophila* due to flagellin (FlaA)-mediated activation of the NAIP5/NLRC4 inflam-
132 masome [23,24]. Thus, to study FlaA-independent host responses within C57Bl/6 mice, we lev-
133 erage FlaA-deficient *L. pneumophila* (Δ*flaA*) strains. We found that *L. pneumophila* Δ*flaA*Δ*legC4*
134 (herein called ΔΔ) mutant strains outcompeted parental Δ*flaA* strains in the lungs of C57Bl/6 wild-
135 type (WT) mice [20] but a growth phenotype for *L. pneumophila* ΔΔ was only observed within
136 cultured mouse primary bone marrow-derived macrophages (BMDMs) activated with exogenous
137 recombinant (r)TNF or rIFN-γ [20]. However, autocrine and paracrine TNF produced by cultured
138 BMDMs is sufficient to attenuate *L. pneumophila* strains induced to overexpress *legC4* from a

139 complementing multicopy plasmid in naïve WT BMDMs [20]. Importantly, this phenotype was
140 specific to intracellularly growing bacteria since *L. pneumophila* growth in broth *in vitro* is unaf-
141 fected by overexpression of *legC4* [20]. Thus, LegC4 confers a growth defect on *L. pneumophila*
142 in a dose-dependent manner within cytokine-activated macrophages.

143 We confirmed our previous results and found that overexpression of *legC4* was sufficient
144 to impair *L. pneumophila* replication within WT BMDMs since *L. pneumophila* ΔΔ (p*legC4*) repli-
145 cation was significantly attenuated compared to both the *L. pneumophila* Δ*flaA* parental strain and
146 *L. pneumophila* ΔΔ harboring an empty plasmid vector (pEV) (**Fig 1A**). Impaired replication was
147 dependent on TNF signaling since overexpression of *legC4* did not impair growth within BMDMs
148 unable to produce TNF (*Myd88*$^{-/-}$; **Fig 1B**) or signal through TNFR1 (*Tnfr1*$^{-/-}$; **Fig 1C**). IFN-γ sig-
149 naling is sufficient for LegC4 restriction [20]; however, the LegC4 restriction phenotype was re-
150 tained within *Ifngr1*$^{-/-}$ BMDMs (**Fig 1D**), indicating that the relatively low levels of IFN-γ secreted
151 by macrophages are not sufficient for restriction. Importantly, we found that LegC4 restriction is
152 not specific to mouse macrophages since both *L. pneumophila* Δ*flaA* and ΔΔ (p*legC4*) were im-
153 paired for replication compared to the ΔΔ (pEV) strain in PMA-differentiated human THP-1 mac-
154 rophages (**Fig 1E**). Thus, LegC4 confers a dose-dependent virulence defect on *L. pneumophila*
155 within mouse and human macrophages.

156 Cytokine signaling drives LegC4 growth defects in cultured BMDMs, but the role of cyto-
157 kine signaling *in vivo* is unclear. We evaluated bacterial fitness by calculating competitive index
158 values for mice infected with a 1:1 mixture of *L. pneumophila* Δ*flaA* and either *L. pneumophila* ΔΔ
159 (pEV) or ΔΔ (p*legC4*) for 48 h (see *Materials & Methods*). We confirmed our previous results
160 showing that LegC4 confers a dose-dependent fitness defect on *L. pneumophila* in the lungs of
161 WT mice since *L. pneumophila* Δ*flaA* was outcompeted by *L. pneumophila* ΔΔ (pEV) but was able
162 to outcompete *L. pneumophila* ΔΔ (pJB*legC4*; **Fig 1F**) [20]. We also confirmed that loss of TNFR1
163 is insufficient to abolish the *legC4* mutant fitness advantage (**Fig 1F**) and obtained similar results

164 in the lungs of IFNGR1- and MyD88-deficient mice (**Fig 1F**). However, the fitness phenotype
165 associated with loss LegC4 was less pronounced in the lungs of *Myd88*$^{-/-}$ mice compared to WT,
166 *Tnfr1*$^{-/-}$ and *Ifngr1*$^{-/-}$ mice (**Fig 1F**), which is likely due to the relatively low levels of MyD88-
167 indpendent IFN-γ produced in the *L. pneumophila*-infected lung [25]. Furthermore, the fitness dis-
168 advantage associated with overexpression of *legC4* was less pronounced in the lungs of MyD88-
169 , IFNGR1- and TNFR1-deficient mice compared to WT mice (**Fig 1F**). These data support our
170 previous work showing that LegC4 augments redundant cytokine-mediated pathogen restriction
171 mechanisms [20]. Overexpression of *legC4* is clearly not necessary to observe a phenotype; how-
172 ever, based on the narrow phenotypic window in BMDMs activated with exogenous cytokine, this
173 infection model is useful for our goal to define how LegC4 potentiates cytokine-mediated re-
174 striction within macrophages
175
176 **LegC4 induces robust phagolysosomal fusion with LCVs BMDMs.** LegC4 attenuates *L.*
177 *pneumophila* replication within cytokine-activated BMDMs; however, the mechanism of bacterial
178 restriction is unknown. Cytokine signaling enhances phagolysosomal fusion with intracellular
179 pathogens [26–29]; thus, we tested the hypothesis that LegC4 restriction involves lysosomal tar-
180 geting of *L. pneumophila*. Virulent *L. pneumophila* establish a replication-permissive compartment
181 called the *Legionella*-containing vacuole (LCV) by blocking endocytic maturation of their phago-
182 some [30,31]. Avirulent Dot/Icm-deficient *L. pneumophila* (Δ*dotA*) are unable to establish a repli-
183 cative LCV and phagosomes rapidly mature to endolysosomes, as evidenced by presence of
184 lysosomal membrane protein LAMP1 [30]. We initially tested the hypothesis that LegC4 induces
185 phagolysosomal fusion with LCVs by blinded immunofluorescence scoring of LAMP1^{+} LCVs
186 within BMDMs infected with *L. pneumophila* strains for 9h. Using our *legC4* overexpression
187 model, we observed robust LegC4-dependent phagolysosomal fusion with significantly more
188 LAMP1^{+} *L. pneumophila* ΔΔ (p*legC4*) LCVs were noted relative to both *L. pneumophila* Δ*flaA* or
189 ΔΔ (pEV) control strains (**Fig 2A**). Strikingly, the abundance of LAMP1^{+} LCVs within WT BMDMs

190 infected with *L. pneumophila* ΔΔ (p*legC4*) did not differ from cells infected with the avirulent Δ*dotA*
191 control strain (**Fig 2A**). Moreover, robust LegC4-mediated phagolysosomal fusion with LCVs was
192 significantly suppressed within TNFR1-deficient BMDMs (**Fig 2A**) since *Tnfr1*$^{-/-}$ BMDMs infected
193 with *L. pneumophila* ΔΔ (p*legC4*) harbored significantly fewer LAMP1^{+} LCVs than those infected
194 with the Δ*dotA* control strain (**Fig 2A**). Interestingly, loss of TNFR1-mediated signaling did not
195 fully abolish phagolysosomal fusion with *L. pneumophila* ΔΔ (p*legC4*) LCVs, but our growth curve
196 data suggest that this is not sufficient for detectable differences in intracellular replication (**Fig**
197 **1C**).

198 Since endogenous LegC4 suppresses *L. pneumophila* replication within BMDMs activated
199 with exogenous rTNF [20], we hypothesized that endogenous LegC4 would also be sufficient to
200 induce phagolysosomal fusion with LCVs in rTNF-treated BMDMs. Indeed, more LAMP1^{+} LCVs
201 were present in rTNF-treated BMDMs infected with *L. pneumophila* Δ*flaA* compared to *L. pneu-*
202 *mophila* ΔΔ (**Fig 2B**). Together, these data show that LegC4 augments phagolysosomal fusion
203 with LCVs in cytokine-activated BMDMs.

204

205 **Pharmacological inhibition of the H^{+}-type vacuolar (v)ATPase abolishes LegC4 restriction**
206 **in BMDMs**. We subsequently tested whether lysosomal acidification contributes to LegC4-medi-
207 ated restriction by quantifying *L. pneumophila* replication within BMDMs treated with Bafilomycin
208 A1 (BAF). BAF is a pharmacological inhibitor of the H^{+}-type vacuolar (v)-ATPase, which drives
209 vacuolar acidification and phagolysosomal fusion [32]. Thus, we tested a role for vATPase activity
210 in LegC4 restriction by quantifying *L. pneumophila* replication within BAF-treated BMDMs. LCV
211 acidification is important for late stages of the *L. pneumophila* lifecycle [33]; however, intracellular
212 replication is minimally impacted within BMDMs treated with a low concentration (≤12.5 nM) of
213 BAF [34]. We found that *L. pneumophila* ΔΔ (p*legC4*) replication did not differ from *L. pneumophila*
214 Δ*flaA* and ΔΔ (pEV) strains within BMDMs treated with 10 nM BAF (**Fig 2C, left**). However, as
215 expected, *L. pneumophila* ΔΔ (p*legC4*) replication was significantly attenuated compared to Δ*flaA*

216 and ΔΔ (pEV) within vehicle (DMSO)-treated BMDMs (**Fig 2C, right**). These data further support
217 a role for lysosomes in LegC4-mediated restriction.
218
219 **LegC4 interacts with host proteasome activator (PA)28α**. To gain insight into the mechanism
220 of LegC4 function, we identified LegC4 binding partners by yeast two-hybrid (Y2H) using LegC4
221 as bait and 30,000 clones of fragmented genomic (g)DNA from mouse splenocytes as prey (Hy-
222 brigenics, Inc., see *Materials & Methods*). Our screen revealed interactions between LegC4 and
223 several regulators of eukaryotic proteasomes, including proteasome activator (PA)28α, PA28γ,
224 and Ecm29 (**Table S1**). The highest-confidence interactor was PA28α with 28 individual clones,
225 all of which encoded a minimal overlapping region in the PA28α C-terminal domain (amino acid
226 residues 105-249) (**Table S1**; **Fig S1**). These data suggest a direct interaction between LegC4
227 and PA28α, which is conserved in amoebae and upregulated by cytokine signaling in macro-
228 phages.
229 We sought to validate our Y2H data using reciprocal affinity purification, co-immunopre-
230 cipitation (IP), and confocal microscopy. We evaluated direct binding between recombinant
231 PA28α and LegC4 by reciprocal affinity chromatography on GST- or His_6-Myc-tagged fusion pro-
232 teins produced in *E. coli.* Using glutathione agarose beads, we found that GST-LegC4 retained
233 Myc-PA28α (**Fig 3A**) and GST-PA28α retained Myc-LegC4 (**Fig 3B**). PA28α did not interact with
234 either GST alone or the unrelated *L. pneumophila* effector Lgt1 (**Fig 3A-B**), known to target eu-
235 karyotic elongation factor 1A [35,36], which indicates that PA28α does not bind non-specifically
236 to *L. pneumophila* effectors. To determine if PA28α and LegC4 interact in mammalian cells, we
237 co-transfected HEK293T cells to transiently produce epitope-tagged 3xFLAG-LegC4 and either
238 PA28α-Myc or GFP-PA28α fusion proteins. Ectopic expression of PA28α was necessary in these
239 experiments since it is expressed only in response to cytokine signaling [37,38]. Using α-FLAG
240 and α-GFP pull-downs, we found that PA28α-Myc co-immunoprecipitated with 3xFLAG-LegC4

241 (**Fig 3C**) and that 3xFLAG-LegC4 co-immunoprecipitated with GFP-PA28α (**Fig 3D**), respectively.
242 Together, these data show that LegC4 binds PA28α.

243 We further evaluated the biological relevance of LegC4-PA28α binding by evaluating pro-
244 tein localization in cells by confocal microscopy. Ectopically produced 3xFLAG-LegC4 co-local-
245 ized with GFP-PA28α within transiently transfected HeLa cells since calculated Pearson Correla-
246 tion Coefficients (PCC) indicated a significant positive correlation between 3xFLAG-LegC4 and
247 GFP-PA28α (Mean PCC = 0.798 ± 0.054) compared to 3xFLAG-LegC4 and GFP (Mean PCC =
248 0.546 ± 0.196) (**Fig 3E-F**). Interestingly, LegC4 modulated PA28α subcellular localization since
249 GFP-PA28α localized to the nucleus in the absence of LegC4 (**Fig 3E**; **Fig 3G, arrowheads**) but
250 was cytosolically localized within cells co-expressing LegC4 **(Fig 3E; Fig 3G, arrows**) [39]. We
251 subsequently tested whether PA28α localization is influenced by Dot/Icm-translocated LegC4
252 within *L. pneumophila*-infected BMDMs. WT BMDMs were infected with *L. pneumophila* Δ*flaA*,
253 ΔΔ, or Δ*dotA* for 7.5 h, at which time a replication-competent LCV is established. Fixed cells were
254 permeabilized and stained with α-*L. pneumophila* and α-PA28α antibodies and Hoechst (DNA)
255 and imaged by confocal microscopy. Endogenous PA28α is constitutively produced in immune
256 cells so can be imaged in BMDMs. We found that PA28α was primarily cytosolic within BMDMs
257 infected with *L. pneumophila* Δ*flaA*, but localized robustly to the nucleus of BMDMs infected with
258 either *L. pneumophila* ΔΔ or Δ*dotA* (**Fig 3H, white arrowheads**). Interestingly, we PA28α was
259 present on LCVs harboring *L. pneumophila* ΔΔ but not Δ*flaA* or Δ*dotA* control strains (**Fig 3H,**
260 **blue arrowheads and inset**). Although altered PA28α localization mediated by translocated
261 LegC4 in naïve infected BMDMs was not sufficient for LegC4 restriction or phagolysosomal fusion
262 in naïve WT BMDMs (Fig 1A, Fig 2B), these data further support a biologically relevant interaction
263 between LegC4 and PA28α, which has not previously identified as a target of bacterial effectors.
264

265 **LegC4 restriction phenotypes are suppressed in PA28α-deficient BMDMs.** Based on the
266 interaction between PA28α and LegC4, we tested the hypothesis that PA28α contributes to
267 LegC4-mediated restriction of *L. pneumophila*. PA28α-deficient (*Psme1*$^{-/-}$) mice are not commer-
268 cially available, so we evaluated the role of PA28α using BMDMs derived from commercially-
269 available PA28αβ-deficient (*Psme1/2*$^{-/-}$) mice [5]. PA28α associates with PA28β to form the
270 PA28αβ (11S) proteasome regulator [40]. PA28β is homologous to PA28α but is dependent on
271 PA28α for activity and is hypothesized to enhance the interaction of PA28α with 20S proteolytic
272 proteasome core particles (CPs) [41]. Thus, we evaluated the role of PA28α in LegC4 restriction
273 in BMDMs and *in vivo* using *Psme1/2*$^{-/-}$ mice. We first tested whether loss of PA28αβ relieves the
274 LegC4-mediated growth attenuation within TNF-activated BMDMs. In agreement with our previ-
275 ous work, *L. pneumophila* Δ*flaA* growth was significantly impaired relative to *L. pneumophila* ΔΔ
276 in rTNF-activated WT BMDMs (*P*=0.015); however, growth of *L. pneumophila* Δ*flaA* and ΔΔ did
277 not differ significantly within *Psme1/2*$^{-/-}$ BMDMs (*P*=0.10; **Fig 4A)**. Moreover, overexpression of
278 *legC4* was insufficient to significantly impair *L. pneumophila* replication within naïve *Psme1/2*$^{-/-}$
279 BMDMs (*P*=0.15) whereas replication was substantially diminished within WT BMDMs (*P*=0.006;
280 **Fig 4B**). Although replication of LegC4-producing bacteria was modestly attenuated in naïve and
281 rTNF *Psme1/2*$^{-/-}$ BMDMs, the lack of statistical significance and differences relative to WT BMDMs
282 provides evidence that PA28αβ activity contributes to LegC4 growth restriction in cultured mac-
283 rophages.

284 We subsequently tested the hypothesis that PA28αβ contributes to LegC4-mediated
285 phagolysosomal fusion with LCVs (Fig 2). Indeed, there were no differences in the abundance of
286 LAMP1^{+} LCVs within *Psme1/2*$^{-/-}$ BMDMs infected with *L. pneumophila* (p*legC4*) compared to *L.*
287 *pneumophila* Δ*flaA* or ΔΔ (pEV) (**Fig 4C**). PA28ab did not affect phagolysosomal fusion with avir-
288 ulent *L. pneumophila* Δ*dotA* since significantly more LAMP1+ LCVs were present compared to all

289 other strains (**Fig 4C**). Thus, LegC4-mediated phagolysosomal fusion is abolished in the absence
290 of PA28αβ.
291
292 **LegC4 does not confer a fitness disadvantage in the lungs of *Psme1/2*$^{-/-}$ mice.** Since loss of
293 PA28αβ was sufficient to suppress LegC4-mediated growth attenuation and phagolysosomal fu-
294 sion in BMDMs, we hypothesized that LegC4 would not confer a fitness disadvantage on *L. pneu-*
295 *mophila* in the lungs of *Psme1/2*$^{-/-}$ mice. We infected *Psme1/2*$^{-/-}$ mice with a 1:1 mixture of *L.*
296 *pneumophila* ΔΔ (pEV) and Δ*flaA* calculated competitive index values from lung homogenates at
297 48 h post-infection. Strikingly, *L. pneumophila* fitness was unaffected by LegC4 in the lungs of
298 *Psme1/2*$^{-/-}$ mice (CI=1.09 ± 0.793); **Fig 4D**). In aggregate, our data suggest that PA28αβ is im-
299 portant for LegC4-mediated restriction in cytokine activated BMDMs and the mouse lung *in vivo.*
300
301 **The abundance of carbonylated proteins in macrophages is increased in the presence of**
302 **LegC4 under oxidative stress conditions.** PA28αβ is expressed constitutively in cells of the
303 innate immune system and upregulated to maintain the integrity of the proteome under oxidative
304 stress conditions [2,38,40,42]. PA28αβ engages proteolytic proteasome 20S core particles (CPs)
305 to promote rapid ubiquitin-independent proteolysis of oxidant-damaged (carbonylated) proteins
306 [4,43], the abundance of which increases commensurately with the abundance reactive oxygen
307 species (ROS) [44,45]. 20S CPs can degrade carbonylated proteins, but their efficiency is sub-
308 stantially increased when in complex PA28αβ [2,43]. Concomitantly, there is a strong negative
309 correlation between PA28αβ activity and carbonylated protein abundance under oxidative stress
310 conditions [43]. Our Y2H data suggest that LegC4 binds the C-terminal domain of PA28α, which
311 is important for PA28αβ docking on proteasome CPs [46–48]. Thus, we rationalized that carbonyl-
312 ated proteins would be more abundant in the presence of LegC4 under oxidative stress condi-
313 tions. To directly evaluate LegC4, we generated RAW 264.7 cells stably transfected with 3xFLAG-

314 LegC4 (RAW-LegC4) or empty plasmid vector (RAW-Cntrl). We confirmed 3xFLAG-LegC4 pro-
315 duction by confocal microscopy (**Fig 5A**) and Western blot (**Fig 5B**). Immunoprecipitation was
316 necessary to visualize LegC4 since it is produced by macrophages at low abundance. However,
317 the abundance of ectopically produced LegC4 was sufficient to attenuate replication of *L. pneu-*
318 *mophila* Δ*flaA* (**Fig 5C**). Attenuated growth was observed at 48 h post-infection, similar to the
319 kinetics of LegC4 restriction within BMDMs (see Fig 1A), which corroborates our microscopy data
320 suggesting that ectopically-produced LegC4 is functional (see Fig 3G-H) and demonstrates that
321 RAW-LegC4 cells are suitable to evaluate LegC4 activity. RAW-LegC4 and -Cntrl cells were in-
322 cubated in the presence or absence of 10 μM H_2O_2 for 24 h and protein carbonyls in cell lysates
323 were quantified by ELISA. We used H_2O_2 since it is membrane permeable, stable in solution, and
324 biologically relevant since *L. pneumophila*-infected macrophages in the lung would also be ex-
325 posed to neutrophil-generated extracellular ROS [26,49]. Indeed, H_2O_2-treated RAW-LegC4 cells
326 contained significantly more protein carbonyls than RAW-Cntrl cells (**Fig 5D**). Under native con-
327 ditions, the concentration of carbonylated proteins was unaffected by LegC4 (**Fig 5D**), which sug-
328 gests that LegC4 does not itself induce oxidative stress. The abundance of protein carbonyls was
329 unaffected by H_2O_2 in RAW-Cntrl cells, likely because upregulation of PA28αβ over the duration
330 of this experiment was sufficient for turnover of damaged proteins.

331 We subsequently tested whether LegC4 increases the abundance of protein carbonyls
332 within *L. pneumophila*-infected BMDMs. *Tnfr1*$^{-/-}$ BMDMs were used to control for any LegC4-me-
333 diated differences in TNF secretion [20] and, consequently, intracellular ROS production [50].
334 *Tnfr1*$^{-/-}$ BMDMs were infected with *L. pneumophila* Δ*flaA*, ΔΔ (pEV), or ΔΔ (p*legC4*) for 4 h in the
335 presence or absence of 50 μM H_2O_2 and protein carbonyls were quantified by Western blot and
336 densitometry. We found that carbonylated proteins were more abundant within BMDMs infected
337 with *L. pneumophila* ΔΔ (p*legC4*) compared to *L. pneumophila* Δ*flaA* and ΔΔ (pEV)-infected and
338 uninfected BMDMs when oxidative stress was induced with H_2O_2 (**Fig 5E-F**). The abundance of
339 protein carbonyls was not affected by LegC4 within naïve untreated BMDMs, which further

340 suggests that LegC4 itself does not induce oxidative stress. Protein carbonyl abundance was not
341 affected by either LegC4 or *L. pneumophila* infection within untreated (UT) BMDMs (**Fig 5E-F**),
342 likely because the amount ROS produced in response to *L. pneumophila* infection under these
343 conditions is insufficient for detectable differences in protein carbonyls by Western blot. Together,
344 these data support our hypothesis that LegC4 perturbs proteostasis in macrophages under oxi-
345 dative stress conditions and suggest that LegC4 may function by impairing PA28αβ activity.
346
347 **Oxidative stress is sufficient for LegC4 restriction in PA28αβ-producing BMDMs.** Our cur-
348 rent data suggest role(s) for PA28αβ and oxidative stress in LegC4 restriction; thus, we hypothe-
349 sized that oxidative stress would be sufficient for LegC4-mediated restriction within BMDMs pro-
350 ducing PA28αβ. To test this, we quantified replication of *L. pneumophila* Δ*flaA* and ΔΔ within WT
351 and *Psme1/2*$^{-/-}$ BMDMs treated with 20 μM H_2O_2 to induce oxidative stress. Indeed, oxidative
352 stress was sufficient for LegC4 restriction since *L. pneumophila* ΔΔ replicated to significantly
353 higher levels than *L. pneumophila* Δ*flaA* in WT BMDMs (**Fig 6A**), showing that oxidative stress is
354 sufficient for LegC4 restriction. Importantly, the growth advantage associated with Δ*legC4* muta-
355 tion was abolished in PA28αβ-deficient BMDMs, but replication of LegC4-producing bacteria was
356 unaffected (**Fig 6A**). These data show that LegC4 impairs *L. pneumophila* replication under oxi-
357 dative stress conditions via a mechanism involving PA28αβ.
358
359 ***L. pneumophila* replication is impaired in *Psme1/2*$^{-/-}$ BMDMs irrespective of LegC4.** Our data
360 suggest that LegC4 restriction is mediated by subversion of PA28αβ. Thus, it's possible that the
361 dose-dependency of LegC4 in naïve BMDMs results from stoichiometric differences in its abun-
362 dance relative to PA28αβ. Thus, we rationalized that *L. pneumophila* replication would be sup-
363 pressed in naïve *Psme1/2*$^{-/-}$ BMDMs irrespective of LegC4 and found that, indeed, both *L. pneu-*
364 *mophila* Δ*flaA* and ΔΔ strains were attenuated for replication within *Psme1/2*$^{-/-}$ BMDMs (**Fig 6B**).

365 Importantly, impaired replication in *Psme1/2*$^{-/-}$ BMDMs was independent of LegC4 since *L. pneu-*
366 *mophila* Δ*flaA* and ΔΔ were equally attenuated (**Fig 6B**). These data show that PA28αβ-deficient
367 macrophages are more restrictive restriction to *L. pneumophila* and suggest a novel role for
368 PA28αβ in host defense against intracellular pathogens in macrophages.
369
370 **Neither TNF production nor cytotoxicity are potentiated by loss of PA82αβ in *L. pneumoph-***
371 ***ila*-infected BMDMs.** Our data suggest that LegC4 enhances phagolysosomal fusion with LCVs
372 via subversion of PA28αβ activity and that loss of PA28αβ is sufficient to impair L. pneumophila
373 intracellular replication. However, impaired bacterial growth may also result from increased TNF
374 production or death of infected BMDMs. We quantified TNF in the supernatants of WT and
375 *Psme1/2*$^{-/-}$ BMDMs infected with *L. pneumophila* Δ*flaA*, ΔΔ (pEV), ΔΔ (p*legC4*) and Δ*dotA* (nega-
376 tive control). At 8h post-infection, there was a modest but statistically significant decrease in TNF
377 secretion from *Psme1/2*$^{-/-}$ BMDMs infected with *L. pneumophila* ΔΔ (p*legC4*) (P=0.049) but no
378 other PA28αβ-mediated differences were observed (**Fig S2A**). At 24 h post-infection, significantly
379 less TNF was present in supernatants of *Psme1/2*$^{-/-}$ BMDMs infected with *L. pneumophila* Δ*flaA*
380 or ΔΔ (pEV) compared to WT BMDMs but no differences in secretion from BMDMs infected with
381 *L. pneumophila* ΔΔ (p*legC4*) (**Fig S2B**). Furthermore, viability of *L. pneumophila*-infected was not
382 affected by either LegC4 or PA28αβ since there were no differences in lactate dehydrogenase
383 (LDH) activity in culture supernatants (**Fig S3**). These data suggest neither LegC4 nor PA28αβ
384 restriction phenotypes result from increased TNF production or death of infected BMDMs.
385
386 **Inflammasome activation is dispensable for LegC4-mediated restriction.** Our data suggest
387 that LegC4 perturbs proteostasis and potentiates oxidative stress. Sustained oxidative and pro-
388 teotoxic stress and proteostasis perturbations can activate the NLRP3 inflammasome, which cul-
389 minates in activation of caspase-1, an effector caspase responsible for pyroptotic cell death and

390 inflammatory cytokine secretion. However, pharmacological inhibition of the NLRP3 inflam-
391 masome with MCC950 did not affect LegC4 restriction since *L. pneumophila* ΔΔ (p*legC4*) was still
392 attenuated for replication compared to *L. pneumophila* ΔΔ (pEV) and Δ*flaA* within WT BMDMs
393 (**Fig S4A**). We also found that LegC4 restriction was preserved within BMDMs derived from
394 caspase-1-deficient (*Casp1*$^{-/-}$) mice (**Fig S4B**). Within cultured macrophages, pyroptotic cell death
395 is responsible for *L. pneumophila* restriction downstream of inflammasome activation. Our data
396 suggest that LegC4 does not enhance LDH release from infected BMDMs (**Fig S3**); however,
397 pyroptotic cell death is more pronounced within BMDMs primed with toll-like (TLR) receptor ago-
398 nists [51,52]. Since TLR2 is important for host defense against *L. pneumophila* [25], we evaluated
399 LDH release from *L. pneumophila*-infected BMDMs pretreated with the TLR2 agonist PAM_3CSK_4.
400 Similar to our previous results (**Fig S3**), LDH release from BMDMs primed with PAM_3CSK_4 was
401 unaffected by LegC4 (**Fig S4C**). These data suggest that LegC4-mediated restriction occurs in-
402 dependently of NLRP3- and caspase-1-dependent pyroptotic cell death and support an overarch-
403 ing model whereby subversion of PA28αβ by LegC4 augments lysosomal pathogen killing under
404 inflammatory and oxidative stress conditions.
405

406 **Discussion**

407 The Dot/Icm effector LegC4 is *bona fide L. pneumophila* virulence factor in a natural host amoeba
408 but confers a dose-dependent fitness disadvantage on *L. pneumophila* in cytokine-activated mac-
409 rophages and in a mouse model of Legionnaires' Disease [20,21]. LegC4 restriction represents a
410 unique mode of effector-mediated immunity since its activity augments existing inflammatory re-
411 sponses in macrophages. In this study, we have uncovered mechanistic insights into LegC4 re-
412 striction and a new role for PA28αβ in cell-autonomous host defense against *L. pneumophila*. We
413 propose a model whereby subversion of host PA28αβ by LegC4 perturbs proteostasis under ox-
414 idative stress conditions, resulting in increased lysosome biogenesis and phagolysosomal fusion

415 with LCVs (**Fig S5**). This model is supported by our data showing that (1) LegC4 enhances cyto-
416 kine-mediated phagolysosomal fusion with LCVs; (2) LegC4 binds and modulates the subcellular
417 localization of PA28α; (2) PA28αβ is required for the effects of LegC4 in BMDMs and *in vivo*; (3)
418 PA28αβ substrates are more abundant in the presence of LegC4; (4) oxidative stress is sufficient
419 for LegC4 restriction; and (5) loss of PA28αβ was restrictive to *L. pneumophila* irrespective of
420 LegC4. This work is the first to identify PA28α as a target for a bacterial effector protein and a
421 role for PA28αβ in innate and effector-mediated host defense against an intracellular bacterial
422 pathogen.
423
424 *L. pneumophila* is an accidental pathogen of humans that rarely transmits between infected indi-
425 viduals. Thus, an evolutionary basis for the LegC4-PA28α interaction can be explained by LegC4
426 targeting the PA28α homolog in amoebae. Indeed, the natural host *A. castellanii*, in which loss of
427 *legC4* confers a growth defect [21], encodes a PA28α homolog (*Ac*PA28) that shares 34% identity
428 with mouse PA28α. Sequence identity between PA28α and *Ac*PA28 is primarily in the PA28α C-
429 terminal domain, which is important for engaging 20S CPs and was contained in all PA28α clones
430 identified in our Y2H screen (**Table S1**). Since PA28αβ substrates were more abundant in the
431 presence of LegC4 (**Fig 5**), we postulate that LegC4 binding impairs PA28-CP complex formation.
432 The function of *Ac*PA28 has not been described; however, it is likely a proteasome regulator
433 based on structural studies showing that mammalian PA28α and evolutionary distant PA28s are
434 similar and all associate with 20S CPs [47,48]. The benefit of inhibiting PA28 in the natural host
435 is unclear, but sequestering PA28 from CPs may preserve the integrity of the constitutive 26S
436 proteasome, a central player in *L. pneumophila*'s virulence strategy [53]. We are currently inves-
437 tigating the molecular mechanism by which LegC4 modulates PA28 activity and its role in *L.*
438 *pneumophila* virulence in natural host amoebae.
439

440 Virulent *L. pneumophila* establish a replicative LCV by avoiding endosomal maturation of their
441 phagosome. The current dogma dictates that lysosomal fusion with LCVs at early time points
442 during infection (≤ 16 h) and *L. pneumophila* intracellular replication are mutually exclusive
443 [33,54]. We found that plasmid expression of *legC4* increased the abundance of LAMP1 on LCVs
444 in within WT BMDMs, similar to what is seen for the avirulent Dot/Icm-deficient strain. LegC4-
445 mediated phagolysosomal fusion was suppressed in *Tnfr1*$^{-/-}$ BMDMs, but significantly more
446 LAMP1+ LCVs were present relative to cells infected with *L. pneumophila* Δ*flaA* and ΔΔ (pEV)
447 control strains. This is intriguing since plasmid expression of *legC4* does not affect *L. pneumophila*
448 replication within *Tnfr1*$^{-/-}$ BMDMs [20] (**Fig 1D**). Based on our model that phagolysosomal fusion
449 results from oxidative stress (**Fig S5**), we postulate that the TNFR1-independent increase in
450 LAMP1+ LCVs within in cells infected with the *legC4* overexpressing strain may result from ROS
451 produced in response to phagocytosis or pattern-recognition receptor signaling [55,56]. A poten-
452 tial explanation for this is that LegC4 may target other host proteins when PA28α is absent, such
453 Ecm29 or PA28γ, which were identified in our Y2H screen (**Table S1**). Ecm29 is a particularly
454 interesting candidate since it disassembles 26S proteasomes under oxidative stress conditions
455 to liberate free 20S CPs that can then associate with PA28αβ [57–59]. This may also explain the
456 modest and non-significant LegC4-mediated growth attenuation retained in *Psme1/2*$^{-/-}$ BMDMs
457 (**Fig 4A-B**). Interestingly, robust phagolysosomal fusion with LCVs was not observed in *Psme1/2*$^{-}$
458 $^{/-}$ BMDMs although these cells are restrictive to *L. pneumophila* (**Fig 6B**). A potential explanation
459 for this observation is that less TNF is produced by *L. pneumophila* ΔΔ (p*legC4*)-infected *Psme1/2*$^{-}$
460 $^{/-}$ BMDMs compared to WT BMDMs (**Fig S2**), although this is unlikely to account for loss of LegC4
461 growth restriction since phenotypes are apparent in rTNF-treated BMDMs (**Fig 4A**). A mechanistic
462 connection between PA28αβ and phagolysosomal fusion can be explained by a compensatory
463 upregulation of lysosome biogenesis and degradation pathways resulting from impaired pro-
464 teasome activity and oxidative stress [3,60,61]. Our data suggest that lysosomes are central to

465 LegC4 restriction, but the underlying mechanism(s) of phagolysosomal fusion with LCVs and bac-
466 terial killing remain to be fully elucidated.
467
468 Lysosomal degradation pathways, including autophagy, are cytoprotective under inflammatory
469 and oxidative stress conditions and central to cytokine-mediated cell-autonomous pathogen re-
470 striction. Lysosomal restriction within IFN-γ-activated macrophages involves immunity-related
471 GTPases (IRGs), which localize to and facilitate lysosomal trafficking to pathogen-containing
472 phagosomes [62]. Although IRGs may contribute to restriction of LegC4-producing *L. pneumoph-*
473 *ila* strains within IFN-γ-activated macrophages [63], IFNGR1 signaling was dispensable for LegC4
474 restriction (Fig 1E-F), which suggests that IRGs are not central drivers of LegC4-mediated *L.*
475 *pneumophila* restriction. It's tempting to speculate that autophagy contributes to LegC4 restriction
476 since autophagy genes are upregulated to clear protein aggregates and protect against TNF-
477 induced death in myeloid cells [64]. Autophagy also prevents aberrant inflammasome-mediated
478 pyroptotic cell death below a certain threshold of inflammasome agonist [65]. The NLRC4 inflam-
479 masome is dispensable for LegC4-mediated restriction [20,21] and we also found no role for the
480 NLRP3 inflammasome (**Fig S4**), which is activated by both oxidative and proteotoxic stress [66].
481 Whether autophagy contributes to LegC4-mediated restriction is unknown and warrants investi-
482 gation since several *L. pneumophila* effectors impair global autophagy in host cells [67–69].
483
484 Using several complementary approaches, we found that LegC4 binds and PA28α and influences
485 its localization in transfected and infected cells. The change in PA28α localization supports an
486 interaction with LegC4, but the underlying mechanism by which it occurs is unclear. We were
487 unable to detect Dot/Icm-translocated LegC4 by confocal microscopy within infected BMDMs,
488 likely because the abundance is below the limit of detection, which is a common challenge in the
489 study of bacterial effectors that do not localize to organellar membranes [70,71]. Our data suggest

490 that the interaction between LegC4 and PA28α may drive localization changes in transfected
491 cells; however, the mechanism is likely more complex since presumed stoichiometric imbalances
492 between PA28α and Dot/Icm-translocated LegC4 make it unlikely that binding is sufficient. Thus,
493 in infected macrophages, LegC4-mediated changes in PA28α localization may result from a need
494 for additional nuclear PA28αβ to clear proteins damaged by the oxidative burst in the presence
495 of LegC4. However, the extent of oxidative damage under these conditions is clearly insufficient
496 to impair *L. pneumophila* replication since endogenous LegC4 does not affect bacterial replication
497 within naïve BMDMs. Interestingly, we also found endogenous PA28α on LCVs harboring LegC4-
498 deficient *L. pneumophila*, which raises the possibilities that LegC4 binding or activity sequesters
499 PA28α in the cytosol away from proteasome complexes associated with the LCV [63,72]. Alt-
500 hough changes in PA28α localization support its functional modulation by LegC4, the molecular
501 underpinnings and consequences of LegC4-PA28α binding, especially based on stoichiometric
502 differences in protein abundance during infection, on PA28ab activity and pathogen restriction
503 require further investigation.
504
505 A role for PA28αβ and oxidative stress in LegC4 restriction was also revealed by the sufficiency
506 of hydrogen peroxide (H_2O_2) for impaired growth in WT BMDMs. H_2O_2 is routinely used to induce
507 oxidative stress in laboratory models since both superoxide ($O_2^{\bullet-}$) and hydroxyl ($OH^{\bullet}$) radicals are
508 unstable in solution. Within immune cells, phagocytosis, pro-inflammatory cytokines, and PRR
509 signaling increase production of ROS by phagocyte NADPH oxidase (NOX2) and mitochondria
510 [50,55,56,73–75]. Intracellular ROS contribute to cell-autonomous pathogen restriction but ROS
511 are also released into the extracellular space via plasma membrane-bound NOX2 or by passive
512 diffusion across membranes (H_2O_2) [49,76]. Interestingly, ROS play a negligible role in host de-
513 fense against *L. pneumophila* in cultured naïve macrophages, likely owing NOX2 exclusion from
514 LCVs [26,77,78]. However, in the lung, ROS are produced abundantly by neutrophils and

515 neutrophil ROS is important for host defense against *L. pneumophila* [26]. Thus, infected alveolar
516 macrophages are exposed to both extracellular ROS produced by lung neutrophils and infection-
517 and cytokine-induced intracellular ROS [49,79,80]. When we treated BMDMs with exogenous
518 H_2O_2 to recapitulate the *in vivo* environment, endogenous LegC4 was sufficient to impair *L. pneu-*
519 *mophila* replication (**Fig 6A**); thus, the fitness disadvantage associated with LegC4 *in vivo* may
520 be due to oxidative stress. Furthermore, it is tempting to speculate that the dose-dependency of
521 LegC4 restriction may correlate with the abundance of ROS. ROS are microbicidal, but this activ-
522 ity is unlikely to be involved in LegC4 restriction since (1) *L. pneumophila* has multiple compli-
523 mentary strategies to protect against oxidative stress and can withstand up to 2 mM H_2O_2 *in vitro*
524 (orders of magnitude greater than intracellular concentrations) [78,81–83]; and (2) replication of
525 LegC4-deficient *L. pneumophila* was unaffected by H_2O_2 treatment (**Fig 6A-B**). While our data do
526 not preclude roles for additional host factors or cytokine-driven cellular processes in LegC4 re-
527 striction of *L. pneumophila*, they support a central role for oxidative stress.
528
529 Our data suggest that oxidative stress is sustained in the presence of LegC4 since oxidatively
530 damaged (carbonylated) proteins were more abundant. Carbonylated proteins are used as a bi-
531 omarker for oxidative stress since proteins and nascent polypeptides are highly susceptible to
532 oxidative damage [44,45]. Importantly, increased protein carbonyl abundance is also indicative of
533 the inability of cellular proteasomes and chaperones to keep pace with the rate of damage [84].
534 Thus, it is conceivable that impaired PA28$\alpha\beta$ activity is indeed responsible for increased protein
535 carbonyl abundance in the presence of LegC4. Nascent polypeptides and misfolded proteins are
536 more susceptible to oxidative damage [85]; thus, impaired co-translational chaperone activity,
537 such as inactivation of Hsp70 by the effector LegK4 [86], may also contribute to carbonylated
538 protein abundance in *L. pneumophila*-infected macrophages. Accumulation of heavily oxidized
539 polypeptides results in formation of aggregates, which are impervious to proteasomal degradation
540 and must be cleared by lysosomal degradation pathways. We think that a global increase in

541 carbonylated proteins drives increased phagolysosomal activity in the presence of LegC4; how-
542 ever, all proteins are not equally susceptible to oxidative damage and individual oxidized species
543 may be involved. For example, the actin cytoskeleton, which plays a critical role in vesicular
544 transport, is deeply influenced by cellular redox status [87]. Filamentous (F)-actin is involved in
545 phagolysosomal fusion with intracellular *L. pneumophila* and pathogen restriction downstream of
546 the caspase-11 inflammasome [88–91]. Caspase-11 promotes phagolysosomal fusion with intra-
547 cellular pathogens by mediating phosphorylation and inactivation of the actin depolymerization
548 factor cofilin [88,91]. Phosphorylated cofilin is highly susceptible to oxidative damage, and its ox-
549 idation may therefore enhance phagolysosomal fusion with LCVs [92].
550
551 In summary, we have uncovered a novel mechanism of effector-mediated host defense and a
552 new role for PA28αβ and oxidative stress in cell-autonomous pathogen restriction. Interestingly,
553 PA28αβ is targeted by several viral pathogens, likely as a means to suppress antigen presentation
554 on MHC class I [93–95]. Impaired antigen presentation is unlikely to play a role in *L. pneumophila*
555 restriction since phenotypes are observed in cultured macrophages and during acute lung infec-
556 tion, prior to initiation of an adaptive immune response. This work is the first to show bacterial
557 pathogen targeting of PA28α and suggest that suppression of PA28αβ activity and aberrant pro-
558 teostasis may be a pathogen-triggered host defense mechanism to potentiate existing inflamma-
559 tory responses. The ability to enhance the antimicrobial potential of activated macrophages has
560 exciting implications for development of host-centric immunotherapeutics and future studies will
561 provide further insight into the ubiquity and mechanism(s) of pathogen restriction induced by pro-
562 teotoxic stress and suppression of PA28αβ activity.
563
564 **Materials & Methods**
565 Bacterial Strains, plasmids, oligonucleotide primers, and reagents.

566 *L. pneumophila* strains, plasmids, and primers used in this study are listed in **Table S2, Table S3,**
567 and **Table S4,** respectively. *L. pneumophila* strains were cultured on supplemented charcoal N-
568 (2-Acetamido)-2-aminoethanesulfonic acid (ACES)-buffered yeast extract (CYE) and grown at
569 37˚C, as described [96]. Liquid cultures were grown overnight with shaking at 37˚C in supple-
570 mented ACES-buffered yeast extract (AYE) medium, as described [20,97]. CYE was supple-
571 mented with 10 µg mL^{-1} chloramphenicol for plasmid maintenance and *legC4* expression was
572 induced with 1 mM isopropyl-β-D-1-thiogalactopyranoside (IPTG; GoldBio) where indicated.
573 *Escherichia coli* strains used for cloning (Top10; Invitrogen) and protein expression [BL21 (DE3);
574 New England Biolabs] were grown at 37 ˚C in Luria-Bertani (LB) medium supplemented with an-
575 tibiotics as appropriate for plasmid selection [50 µg mL^{-1} kanamycin (GoldBio), 25 µg mL^{-1} chlo-
576 ramphenicol (GoldBio), or 100 µg mL^{-1} ampicillin (GoldBio)]. Protein expression in BL21 (DE3)
577 was induced with 1 mM IPTG. Unless otherwise indicated, all chemicals were obtained from Mil-
578 lipore Sigma (St. Louis, MO).
579
580 Mice and bone marrow-derived macrophages
581 Mice on C57BL/6 background were purchased from the Jackson Laboratories (Bar Harbor,
582 Maine). Wild-type, *Tnfr1*$^{-/-}$, *Ifngr1*$^{-/-}$, and *Myd88*$^{-/-}$ mice were purchased from live repositories and
583 *Psme1/2*$^{-/-}$ mice were recovered from cryopreserved embryos and bred for homozygotes at the
584 Jackson Laboratories (Bar Harbor, ME). In-house colonies were maintained in specific pathogen-
585 free conditions at Kansas State University and Michigan State University.
586 Bone marrow was harvested from seven- to twelve-week-old mice as described [98].
587 BMDMs were generated by differentiation in RPMI supplemented with 20% heat-inactivated fetal
588 bovine serum (HI-FBS) (Biowest, Riverside, MO) and 15% L929 cell supernatant for 6 days prior
589 to seeding for infection. Femurs from C57Bl/6 *Casp1*$^{-/-}$ mice were a gift from Dr. Russell Vance
590 (University of California, Berkeley).

591 All experiments involving animals were approved by the Kansas State University and
592 Michigan State University Institutional Animal Care and Use Committees (KSU Protocols: 4022,
593 4501, and 4386; MSU protocol: PROTO202200365) and performed in compliance with the Animal
594 Welfare Act and NIH guidelines. Animals were euthanized in accordance with American Veteri-
595 nary Medical Association Guidelines.
596
597 Competitive Index
598 Six- to twelve-week-old sex- and age-matched mice were anesthetized with ketamine/xylazine
599 and infected via the intranasal route as previously described [20]. Mixed bacterial inoculums (1:1)
600 containing a total of 5 x 10^6 bacteria were diluted and plated on selective medium (10 µg mL^{-1}
601 chloramphenicol for plasmid selection). At 48 h post-infection, mice were euthanized and homog-
602 enates from extracted lung tissue were plated on selective media, as described [20]. CFU were
603 enumerated and used to calculate CI values [$(CFUcm^R_{48h}/CFUwt_{48h})/(CFUcm^R_{IN})/CFUwt_{IN})$].
604
605 Molecular Cloning
606 Plasmids were generated for stable and transient ectopic production in mammalian cells and re-
607 combinant protein production in *E. coli*. For production of 3xFLAG-LegC4, *legC4* was amplified
608 from *L. pneumophila* genomic (g)DNA using LegC4BamHI-F/LegC4NotI-R primer pairs (**Table**
609 **S4**) and cloned as a BamHI/NotI fragment into 3xFLAG 4/TO (**Table S3**) [99]. To produce GFP-
610 PA28α, *psme1* was amplified from pCMV-3Tag-4a::*psme1* (purchased from Genscript, Pisca-
611 taway, New Jersey) using Psme1Sal1-F/Psme1BamHI-R primer pairs (**Table S4**) and cloned as
612 a Sal1/BamH1 fragment into pEGFPC1 (Clontech). For production of GST- and His_6-Myc-fusion
613 proteins, open reading frames were cloned into pGEX-6P-1 and pT7HMT vectors, respectively.
614 *psme1* was PCR-amplified from pCMV-3Tag-4a::*psme1* and *legC4* PCR-amplified from *L. pneu-*
615 *mophila* genomic (g)DNA using primers Psme1-BamHI-F/Psme1-NotI-R and LegC4-BamHI-
616 F3/LegC4-NotI-R, respectively (**Table S4**). Each of the amplified fragments were cloned as a

617 BamHI/NotI fragment into either pGEX-GP-1 or pT7HMT. pGEX::*lgt1* and pT7HMT::*lgt1* were
618 constructed previously [100]. Confirmation of DNA sequences was done by Sanger sequencing
619 (Eton Biosciences Inc.). Plasmid DNA was transformed into chemically competent *E. coli* Top10
620 (Invitrogen) or BL21 (DE3) (New England Biolabs) for plasmid purification and recombinant pro-
621 tein production, respectively. Plasmid DNA was purified for transfection into mammalian cell lines
622 using a ZymoPURE II Plasmid Maxiprep Kit (Zymo Research).
623
624 Recombinant protein production and affinity chromatography
625 *E. coli* BL21 (DE3) overnight cultures were sub-cultured into fresh LB medium containing the
626 appropriate antibiotics at 1:100 and grown with shaking for 3h at 37˚C. Recombinant protein pro-
627 duction was induced with 1mM IPTG and cultures were grown overnight with shaking at 16˚C.
628 Bacteria were harvested by centrifugation at 1,400 r.c.f. for 10 min at 4˚C, washed with ice-cold
629 PBS and incubated in bacterial lysis buffer [50mM Tris pH 8.0, 100mM NaCl, 1mM EDTA, 200µg
630 mL^{-1} lysozyme, and complete protease inhibitor (Roche)] for 30 min on ice followed by addition of
631 2 mM DTT. Bacteria were sonicated and lysates were clarified by centrifugation at 21,000 r.c.f.
632 for 15 min at 4˚C, as described [100]. Clarified lysates harboring GST-fusion proteins were incu-
633 bated with magnetic glutathione agarose beads (Pierce) for 1hr at 4˚C with rotation and washed
634 twice in Glutathione wash buffer [125mM Tris pH 7.4, 250mM NaCl, 1mM DTT, 1mM EDTA].
635 Clarified lysates harboring His_6-Myc-fusion proteins were added to the beads and incubated at
636 4˚C with rotation for 1hr. Beads were washed twice with Glutathione wash buffer and proteins
637 were eluted by boiling in Laemmli sample buffer. Proteins were separated by SDS-PAGE followed
638 by Coomassie brilliant blue staining and Western blot (see below).
639
640 Cell Culture and Transfections
641 HEK 293T, HeLa, and RAW 264.7 cells (gifts from Dr. Craig Roy, Yale University) were main-
642 tained at 37˚C and 5% CO_2 in Dulbecco's Modified Eagle Medium (DMEM) supplemented with

643 10% HI-FBS. THP-1 cells were purchased from the American Type Culture Collection (ATCC)
644 and maintained in RPMI supplemented with 10% HIFBS and differentiated with 100 nM phorbal
645 12-myristate 13-acetate (PMA) for 4 days prior to infection with *L. pneumophila* (see below). All
646 cell lines were used between passage 4-20.

647 HEK 293T cells were transfected with purified plasmid DNA (**Table S2**) for 24 h using
648 calcium phosphate as described [101]. HeLa cells were transfected for 24 h using jetPRIME trans-
649 fection reagent according to manufacturer's guidelines. Two hours before transfection, HeLa cells
650 were washed and incubated in low-serum media (DMEM/4% HIFBS). Media were replaced with
651 DMEM 10% HIFBS four hours post-transfection and assayed 24 h post-transfection.

652 To generate RAW 264.7 cells with stable plasmid integrations, cells were transfected with
653 pcDNA::*3xflag-legC4* or pcDNA::*3xflag* vector (**Table S2**) using a Nucleofector 2b electroporator
654 (Lonza, Basel, Switzerland) and cultured over 14 days with Zeocin selection (200 -1000 µg mL^{-}
655 ^{1}). 3xFLAG-LegC4 expression was confirmed by Western blot and confocal microscopy using a-
656 FLAG antibodies (see below) and stable RAW 264.7 cells were maintained in culture in the pres-
657 ence of 200 µg mL^{-1} Zeocin. For *L. pneumophila* infections, cells were seeded one day prior to
658 infection and infected in the absence of Zeocin.

659

660 <u>Western blot</u>

661 Boiled protein samples were separated by SDS-PAGE and transferred to polyvinylidene difluoride
662 (PVDF) membrane using a BioRad TransBlot semidry transfer apparatus. Membranes were in-
663 cubated in blocking buffer [5% non-fat milk powder dissolved in Tris-buffered saline-0.1% Tween-
664 20 (TBST)]. Primary antibodies [rabbit α-FLAG (Sigma-Aldrich, F1804), rabbit α-Myc (Cell Sig-
665 naling, 2278S), rabbit α-GFP (Abcam, ab6556)] were used at 1:1,000 in blocking buffer and de-
666 tected with horseradish peroxidase (HRP)-conjugated secondary antibodies (1:5,000; Ther-
667 moFisher). Membranes were washed in TBST followed by addition of enhanced

668 chemiluminescent (ECL) reagent (GE Amersham) and visualization using an Azure c300 Dark-
669 room Replacer or a GE Amersham Imager 600.
670
671 Immunoprecipitation
672 Transiently transfected HEK 293T cells or RAW 264.7 cells were washed with phosphate-buffered
673 saline and lysed in ice-cold NP-40 buffer [1% non-iodet P40 (v/v), 20 mM Tris pH 7.5, 150 mM
674 NaCl, 10 mM $Na_4P_2O_7$, 50 mM NaF, complete protease inhibitor (Roche)]. Lysates were clarified
675 and proteins were immunoprecipitated using α-FLAG M2 magnetic beads or protein G-conjugated
676 Dynabeads (ThermoFisher) pre-incubated with rabbit α-GFP antibody (Abcam, ab6556), as indi-
677 cated and according to manufacturer's instructions. Input samples were collected from cell lysates
678 prior to incubation with beads. Beads and input samples were resuspended in 3x Laemmli sample
679 buffer for SDS-PAGE and Western blot analysis.
680
681 Protein carbonyl assays
682 Protein carbonyls were quantified using the OxiSelect Protein Carbonyl ELISA Kit (Cell Biolabs)
683 following manufacturer's instructions. Briefly, RAW 264.7 cells were seeded at $2x10^6$ in a 10 cm
684 tissue culture dishes in DMEM 10% HIFBS. The next day, media were aspirated, and cells were
685 incubated in DMEM/2.5% HIFBS in the presence or absence of 10 μM H_2O_2. After 24 h, cells
686 were washed twice in PBS and lysed in ice-cold 500 μL of detergent-free lysis buffer [25 mM
687 HEPES pH 7.4, 150 mM NaCl, 10 mM $MgCl_2$, 1 mM EDTA, 2% glycerol (v/v)] supplemented with
688 complete protease inhibitor cocktail (Roche). Cell lysates were scraped into a pre-chilled micro-
689 centrifuge tube and incubated with agitation for 30 min at 4˚C followed by sonication at 40% in-
690 tensity three times in 10 second intervals. Lysates were clarified by centrifugation at 4˚C for 20
691 min at 13,000 r.c.f. Supernatants were transferred to a fresh tube, snap frozen in liquid nitrogen
692 for 2 min and stored at -80˚C until use. Protein concentrations were quantified using a Coomassie

693 Plus (Bradford) Protein Assay (Pierce) and diluted to 10 µg mL^{-1}. Samples and standards were
694 adsorbed to a 96-well protein binding plate and ELISA was performed according to manufacturer's
695 instructions. Absorbance at 450 nm was quantified on a BioTek Epoch2 microplate reader.

696 Protein carbonyls were visualized using the OxiSelect Protein Carbonyl Immunoblot Kit
697 (Cell Biolabs). *Tnrf1*$^{-/-}$ BMDMs were seeded in 24-well plates at $2.5x10^5$ one day prior to infection
698 with indicated *L. pneumophila* strains at an MOI of 50 in the presence or absence of 10 µM H_2O_2.
699 One hour after infection, cells were washed 3x with $PBS^{-/-}$, media were replaced and cells were
700 incubated for an additional 3 h in the presence or absence of H_2O_2. Cells were washed in ice-cold
701 PBS and lysed in 120 µL ice-cold NP-40 lysis buffer (see above). Lysates were diluted in 3x
702 Laemmli sample buffer and boiled for 10 min. Proteins were separated on a 4-20% gradient SDS-
703 PAGE gel and transferred to PVDF membrane using a BioRad TransBlot semi-dry transfer appa-
704 ratus. Membranes were processed according to manufacturer's instructions using 10 min wash
705 steps. Blots were stripped and re-probed with rabbit α-β-actin antibody (1:1000; Cell Signaling
706 Technology) followed by goat-α-rabbit-HRP (1:5000; ThermoFisher). Blots were visualized as de-
707 scribed above and densitometry was performed using Fiji ImageJ and Adobe Photoshop software.
708

709 Yeast Two-Hybrid Analysis

710 Yeast two-hybrid screening was performed by Hybrigenics Services, S.A.S., Evry, France
711 (http://www.hybrigenics-services.com). The *legC4* coding sequence was PCR-amplified from
712 pSN85::*legC4* [20] and cloned into pB66 as a C-terminal fusion to Gal4 DNA-binding domain
713 (Gal4-C4). The construct was checked by sequencing and used as a bait to screen a random-
714 primed Mouse Spleen library constructed into pP6. pB66 derives from the original pAS2ΔΔ vector
715 [102] and pP6 is based on the pGADGH plasmid [103].

716 Sixty million clones (6-fold the complexity of the library) were screened using a mating
717 approach with YHGX13 (Y187 ade2-101::loxP-kanMX-loxP, mat-α) and CG1945 (mat-a) yeast

718 strains as previously described [102]. 303 His+ colonies were selected on a medium lacking tryp-
719 tophan, leucine and histidine, and supplemented with 2mM 3-aminotriazole to handle bait auto-
720 activation. The prey fragments of the positive clones were amplified by PCR and sequenced at
721 their 5' and 3' junctions. The resulting sequences were used to identify the corresponding inter-
722 acting proteins in the GenBank database (NCBI) using a fully automated procedure. A confidence
723 score (PBS, for Predicted Biological Score) was attributed to each interaction as previously de-
724 scribed [104].
725
726 Immunofluorescence Microscopy
727 To quantify LAMP1+ LCVs in naïve macrophages, $1x10^5$ BMDMs were seeded on poly-L-lysine
728 (PLL)-coated glass coverslips in 24-well plates and infected with *L. pneumophila* at a multiplicity
729 of infection (MOI) of 25 in triplicates. At 1h post-infection, cells were washed 3x in PBS to remove
730 extracellular bacteria and cells were incubated for an additional 8 h in fresh media was added.
731 Quantification of LAMP1+ LCVs in rTNF-treated BMDMs was performed as described but media
732 were supplemented with 25 ng mL^{-1} rTNF throughout the course of infection, which was allowed
733 to proceed for an additional 5 h after washing in PBS. Coverslips were fixed with 4% paraformal-
734 dehyde (PFA; Thermo Scientific), permeabilized in ice cold methanol, and blocked with blocking
735 buffer [0.1% saponin (w/v), 1% HIFBS (v/v), 0.5% bovine serum albumin (BSA; w/v) in PBS].
736 Coverslips were stained with 1:1,000 rabbit α-*L. pneumophila* (Invitrogen, PA17227), 1:2,000 rat
737 α-LAMP1 (Developmental Studies Hybridoma Bank) primary antibodies and 1:500 Alexa 488-
738 conjugated goat α-rabbit and Alexa594-conjugated goat α-rat secondary antibodies (Ther-
739 moFisher) in blocking buffer. Nuclei were stained with Hoechst (ThermoFisher) at 1:2,000. Co-
740 verslips were mounted on glass slides with ProLong Gold Antifade Mountant (ThermoFisher).
741 LAMP1+ LCVs were scored on a Leica DMiL LED inverted epifluorescence microscope (*n*=300
742 cells/strain) and the researcher scoring the samples were blind to their identity.

743 For confocal microscopy of transfected cells, HeLa cells were seeded on PLL-coated co-
744 verslips and transfected as described above. Coverslips were fixed in 4% PFA and processed as
745 described above using mouse α-FLAG M2 (Sigma; 1:1,000) and rabbit α-GFP (Abcam; ab6556;
746 1:5,000) primary antibodies and Alexa546-conjugated goat α-mouse and Alexa488-conjugated
747 goat α-rabbit antibodies (ThermoFisher; 1:500). Images were captured on a Zeiss LSM-5 PAS-
748 CAL laser scanning confocal microscope (KSU Division of Biology Microscopy Facility). Co-local-
749 ization was scored using the Pearsons algorithm for individual cells (*n*=10) using the colocalize
750 tool Fiji ImageJ software.

751 For confocal microscopy of infected macrophages, $1.5x10^5$ cells were seeded on PLL-
752 coated coverslips and infected as described above. Coverslips were fixed with 4% PFA and pro-
753 cessed as above using rabbit α-*L. pneumophila* (Millipore Sigma; 1:1000) and mouse α-PA28α
754 (SantaCruz; 1:100) primary antibodies, Alexa488-conjugated goat α-rabbit and Alexa594-conju-
755 gated goat α-mouse secondary antibodies, and Hoechst (ThemoFisher; 1,2000). Images were
756 captured using an Olympus FluoView FV1000 confocal Laser scanning microscope (MSU Center
757 for Advanced Microscopy).

758

759 <u>*L. pneumophila* intracellular growth curves</u>

760 To quantify *L. pneumophila* intracellular replication, macrophages were seeded in 24-well tissue
761 culture plates and infected in triplicates at an MOI of 1 the next day. Differentiated BMDMs were
762 seeded at $2.5x10^5$ in seeding media (RPMI, 10% HIFBS, 7.5% L929 cell supernatant), THP-1
763 cells were seeded at $5x10^5$ and differentiated with 100 nM PMA in RPMI 10% HIFBS for three
764 days. Cells were washed with PBS and incubated in the absence of PMA for one day prior to
765 infection. Stable RAW 264.7 cells were seeded at $2.5x10^5$ in DMEM 2.5%HIFBS. At 1 h post-
766 infection, cells were washed 3x with PBS followed by addition of fresh media. Macrophages were
767 lysed in sterile water and colony forming units (CFU) were enumerated at the indicated time points

768 as described [20]. Where indicated, 25 ng mL^{-1} rTNF (Gibco), 20-50 μM H_2O_2 (VWR), 10 nM
769 bafilomycin A1 (BAF; ApexBio), or 1 μM MCC950 (ApexBio) were added at the time of infection
770 and maintained throughout. DMSO was used as a vehicle control where indicated.
771
772 Enzyme-linked immunosorbent assay (ELISA)
773 To quantify TNF secretion, 2.5 x 10^5 BMDMs were seeded in 24-well tissue culture plates and
774 infected with the indicated *L. pneumophila* strains at an MOI of 10. After 1 h of infection, cells
775 were washed with PBS, and media were replaced. Supernatants were at 8 h post-infection and
776 used fresh or stored at -20˚C for up to 1 week and TNF was quantified using mouse TNF-
777 α ELISA MAX kit (BioLegend) following manufacturer's instructions. Absorbance at 450 nm was
778 quantified on a BioTek Epoch2 microplate reader.
779
780 Cytotoxicity assay
781 To quantify cell death, lactate dehydrogenase (LDH) activity in cell supernatants was quantified.
782 BMDMs were seeded in triplicates at 2.5x10^5 in a 24-well tissue culture plate for 24 h and infected
783 with the indicated *L. pneumophila* strains at an MOI of 10 in 500 μL of seeding media (RPMP/10%
784 HIFBS/7.5% L929 cell supernatant) and incubated for the indicated times. Supernatants were
785 transferred to a 96-well plate and centrifuged at 200 r.c.f. for 10 min. LDH was quantified using
786 the CytoTox 96 Non-Radioactive Cytotoxicity Assay (Promega) according to manufacturer's in-
787 structions. Absorbance at 490 nm was quantified on a BioTek Epoch2 microplate reader and
788 percent cytotoxicity was calculated by normalizing absorbance values to cells treated with lysis
789 buffer. Where indicated, cells were primed with 1 μM PAM_3CSK_4 (Tocris) for 24 h prior to infection
790 and plasmid expression of *legC4* was induced with 1 mM IPTG.
791
792 Statistical analysis

793 Statistical analyses were performed with GraphPad Prism 9 software using either Students' *t*-test,
794 or two-way ANOVA, as indicated, with a 95% confidence interval. Data are presented as mean ±
795 standard deviation (s.d.) or standard error of the mean (s.e.m.) and, unless otherwise indicated,
796 statistical analyses were performed on samples in triplicates.
797

798 **Acknowledgements**

799 We thank Dr. Russell Vance for femurs from *Casp1*$^{-/-}$ mice and helpful discussions. We also thank
800 Andrew Haskell for assistance within blinded microscopic scoring of *L. pneumophila*-infected
801 cells. This work was funded by NIH/NIGMS P20GM130448 (to S.R.S.); Kansas-INBRE (K-IN-
802 BRE) Postdoctoral Fellowship P20GM103418 (to D.C.) and Semester Scholar Award (to A.G.S.);
803 Kansas State University Johnson Cancer Research Center Summer Stipend Award (to T.N.) and
804 Faculty Expansion Award (to S.R.S.); and startup funds from Kansas State University and Michi-
805 gan State University (to S.R.S.)
806

807
808 **References**
809

810 1. Mitchell* G, Chen* C, Portnoy DA. Strategies Used by Bacteria to Grow in Macrophages. Mi-
811 crobiol Spectr. 2016;4. doi:10.1128/microbiolspec.mchd-0012-2015

812 2. Pickering AM, Koop AL, Teoh CY, Ermak G, Grune T, Davies KJA. The immunoproteasome,
813 the 20S proteasome and the PA28αβ proteasome regulator are oxidative-stress-adaptive prote-
814 olytic complexes. Biochem J. 2010;432: 585–94. doi:10.1042/bj20100878

815 3. Dikic I. Proteasomal and Autophagy Degradation Systems. Annu Rev Biochem. 2016;86: 1–
816 32. doi:10.1146/annurev-biochem-061516-044908

817 4. Graaf N de, Helden MJG van, Textoris-Taube K, Chiba T, Topham DJ, Kloetzel P-M, et al.
818 PA28 and the proteasome immunosubunits play a central and independent role in the produc-
819 tion of MHC class I-binding peptides in vivo. Eur J Immunol. 2011;41: 926–35.
820 doi:10.1002/eji.201041040

821 5. Preckel T, Fung-Leung W-P, Cai Z, Vitiello A, Salter-Cid L, Winqvist O, et al. Impaired Im-
822 munoproteasome Assembly and Immune Responses in PA28−/− Mice. Science. 1999;286:
823 2162–2165. doi:10.1126/science.286.5447.2162

824 6. Mondino S, Schmidt S, Rolando M, Escoll P, Gomez-Valero L, Buchrieser C. Legionnaires'
825 Disease: State of the Art Knowledge of Pathogenesis Mechanisms of Legionella. Annu Rev Pa-
826 thology Mech Dis. 2019;15: 1–28. doi:10.1146/annurev-pathmechdis-012419-032742

827 7. Hugoson E, Guliaev A, Ammunét T, Guy L. Host-adaptation in Legionellales is 1.9 Ga, coinci-
828 dent with eukaryogenesis. Mol Biol Evol. 2022;39: msac037. doi:10.1093/molbev/msac037

829 8. Gomez-Valero L, Rusniok C, Carson D, Mondino S, Pérez-Cobas AE, Rolando M, et al. More
830 than 18,000 effectors in the Legionella genus genome provide multiple, independent combina-
831 tions for replication in human cells. Proc National Acad Sci. 2019;116: 2265 2273.
832 doi:10.1073/pnas.1808016116

833 9. Park JM, Ghosh S, O'Connor TJ. Combinatorial selection in amoebal hosts drives the evolu-
834 tion of the human pathogen Legionella pneumophila. Nat Microbiol. 2020;4: 599–609.
835 doi:10.1038/s41564-019-0663-7

836 10. Ngwaga T, Chauhan D, Shames SR. Mechanisms of Effector-Mediated Immunity Revealed
837 by the Accidental Human Pathogen Legionella pneumophila. Front Cell Infect Mi. 2021;10:
838 593823. doi:10.3389/fcimb.2020.593823

839 11. Massis LM, Zamboni DS. Innate immunity to legionella pneumophila. Front Microbiol.
840 2011;2: 109. doi:10.3389/fmicb.2011.00109

841 12. Shin S. Innate Immunity to Intracellular Pathogens: Lessons Learned from Legionella pneu-
842 mophila. Adv Appl Microbiol. 2012;79: 43 71. doi:10.1016/b978-0-12-394318-7.00003-6

843 13. Chauhan D, Shames SR. Pathogenicity and Virulence of Legionella: Intracellular replication
844 and host response. Virulence. 2021;12: 1122–1144. doi:10.1080/21505594.2021.1903199

845 14. Lockwood DC, Amin H, Costa TRD, Schroeder GN. The Legionella pneumophila Dot/Icm
846 type IV secretion system and its effectors: This article is part of the Bacterial Cell Envelopes col-
847 lection. Microbiology+. 2022;168. doi:10.1099/mic.0.001187

848 15. Fontana MF, Banga S, Barry KC, Shen X, Tan Y, Luo Z-Q, et al. Secreted bacterial effectors
849 that inhibit host protein synthesis are critical for induction of the innate immune response to viru-
850 lent Legionella pneumophila. Plos Pathog. 2011;7: e1001289. doi:10.1371/journal.ppat.1001289

851 16. Asrat S, Dugan AS, Isberg RR. The frustrated host response to Legionella pneumophila is
852 bypassed by MyD88-dependent translation of pro-inflammatory cytokines. Roy CR, editor. Plos
853 Pathog. 2014;10: e1004229. doi:10.1371/journal.ppat.1004229

854 17. Fischer NL, Naseer N, Shin S, Brodsky IE. Effector-triggered immunity and pathogen sens-
855 ing in metazoans. Nat Microbiol. 2019;5: 14–26. doi:10.1038/s41564-019-0623-2

856 18. Naujoks J, Lippmann J, Suttorp N, Opitz B. Innate sensing and cell-autonomous resistance
857 pathways in Legionella pneumophila infection. Int J Med Microbiol. 2017;308: 161–167.
858 doi:10.1016/j.ijmm.2017.10.004

859 19. Misch EA. Legionella: virulence factors and host response. Curr Opin Infect Dis. 2016;29:
860 280 286. doi:10.1097/qco.0000000000000268

861 20. Ngwaga T, Hydock AJ, Ganesan S, Shames SR. Potentiation of Cytokine-Mediated Re-
862 striction of Legionella Intracellular Replication by a Dot/Icm-Translocated Effector. J Bacteriol.
863 2019;201: e00853-19. doi:10.1128/jb.00755-18

864 21. Shames SR, Liu L, Havey JC, Schofield WB, Goodman AL, Roy CR. Multiple Legionella
865 pneumophila effector virulence phenotypes revealed through high-throughput analysis of tar-
866 geted mutant libraries. Proc National Acad Sci. 2017;63: E10446–E10454.
867 doi:10.1073/pnas.1708553114

868 22. Ghosh S, O'Connor TJ. Beyond Paralogs: The Multiple Layers of Redundancy in Bacterial
869 Pathogenesis. Front Cell Infect Mi. 2017;7: 467. doi:10.3389/fcimb.2017.00467

870 23. Molofsky AB, Byrne BG, Whitfield NN, Madigan CA, Fuse ET, Tateda K, et al. Cytosolic
871 recognition of flagellin by mouse macrophages restricts Legionella pneumophila infection. J Exp
872 Medicine. 2006;203: 1093 1104. doi:10.1084/jem.20051659

873 24. Ren T, Zamboni DS, Roy CR, Dietrich WF, Vance RE. Flagellin-deficient Legionella mutants
874 evade caspase-1- and Naip5-mediated macrophage immunity. Plos Pathog. 2006;2: e18.
875 doi:10.1371/journal.ppat.0020018

876 25. Archer KA, Roy CR. MyD88-Dependent Responses Involving Toll-Like Receptor 2 Are Im-
877 portant for Protection and Clearance of Legionella pneumophila in a Mouse Model of Legion-
878 naires' Disease. Infect Immun. 2006;74: 3325 3333. doi:10.1128/iai.02049-05

879 26. Ziltener P, Reinheckel T, Oxenius A. Neutrophil and Alveolar Macrophage-Mediated Innate
880 Immune Control of Legionella pneumophila Lung Infection via TNF and ROS. Luo Z-Q, editor.
881 Plos Pathog. 2016;12: e1005591. doi:10.1371/journal.ppat.1005591

882 27. Santic M, Molmeret M, Kwaik YA. Maturation of the Legionella pneumophila-containing
883 phagosome into a phagolysosome within gamma interferon-activated macrophages. Infect Im-
884 mun. 2005;73: 3166 3171. doi:10.1128/iai.73.5.3166-3171.2005

885 28. Coers J, Brown HM, Hwang S, Taylor GA. Partners in anti-crime: how interferon-inducible
886 GTPases and autophagy proteins team up in cell-intrinsic host defense. Curr Opin Immunol.
887 2018;54: 93–101. doi:10.1016/j.coi.2018.06.008

888 29. Meunier E, Broz P. Interferon-inducible GTPases in cell autonomous and innate immunity.
889 Cell Microbiol. 2016;18: 168–180. doi:10.1111/cmi.12546

890 30. Roy CR, Berger KH, Isberg RR. Legionella pneumophila DotA protein is required for early
891 phagosome trafficking decisions that occur within minutes of bacterial uptake. Mol Microbiol.
892 1998;28: 663–674. doi:10.1046/j.1365-2958.1998.00841.x

893 31. Swanson MS, Isberg RR. Association of Legionella pneumophila with the macrophage en-
894 doplasmic reticulum. Infection and immunity. 1995;63: 3609 3620.

895 32. Matsumoto N, Nakanishi-Matsui M. Proton pumping V-ATPase inhibitor bafilomycin A1 af-
896 fects Rab7 lysosomal localization and abolishes anterograde trafficking of osteoclast secretory
897 lysosomes. Biochem Bioph Res Co. 2019;510: 421–426. doi:10.1016/j.bbrc.2019.01.118

898 33. Sturgill-Koszycki S, Swanson MS. Legionella pneumophila Replication Vacuoles Mature into
899 Acidic, Endocytic Organelles. J Exp Medicine. 2000;192: 1261–1272.
900 doi:10.1084/jem.192.9.1261

901 34. Khweek AA, Caution K, Akhter A, Abdulrahman BA, Tazi M, Hassan H, et al. A bacterial
902 protein promotes the recognition of the Legionella pneumophila vacuole by autophagy. Eur J
903 Immunol. 2013;43: 1333 1344. doi:10.1002/eji.201242835

904 35. Belyi Y, Niggeweg R, Opitz B, Vogelsgesang M, Hippenstiel S, Wilm M, et al. Legionella
905 pneumophila glucosyltransferase inhibits host elongation factor 1A. Proc National Acad Sci.
906 2006;103: 16953 16958. doi:10.1073/pnas.0601562103

907 36. Belyi Y, Tartakovskaya D, Tais A, Fitzke E, Tzivelekidis T, Jank T, et al. Elongation Factor
908 1A Is the Target of Growth Inhibition in Yeast Caused by Legionella pneumophila Glucosyltrans-
909 ferase Lgt1. J Biol Chem. 2012;287: 26029 26037. doi:10.1074/jbc.m112.372672

910 37. Seifert U, Bialy LP, Ebstein F, Bech-Otschir D, Voigt A, Schröter F, et al. Immunopro-
911 teasomes Preserve Protein Homeostasis upon Interferon-Induced Oxidative Stress. Cell.
912 2010;142: 613–624. doi:10.1016/j.cell.2010.07.036

913 38. Fabunmi RP, Wigley WC, Thomas PJ, DeMartino GN. Interferon gamma regulates accumu-
914 lation of the proteasome activator PA28 and immunoproteasomes at nuclear PML bodies. J Cell
915 Sci. 2001;114: 29–36.

916 39. Soza A, Knuehl C, Groettrup M, Henklein P, Tanaka K, Kloetzel P-M. Expression and sub-
917 cellular localization of mouse 20S proteasome activator complex PA28. Febs Lett. 1997;413:
918 27–34. doi:10.1016/s0014-5793(97)00864-8

919 40. Mott JD, Pramanik BC, Moomaw CR, Afendis SJ, DeMartino GN, Slaughter CA. PA28, an
920 activator of the 20 S proteasome, is composed of two nonidentical but homologous subunits. J
921 Biological Chem. 1994;269: 31466–71.

922 41. Wilk S, Chen W-E, Magnusson RP. Properties of the Beta Subunit of the Proteasome Acti-
923 vator PA28 (11S REG). Arch Biochem Biophys. 2000;384: 174–180.
924 doi:10.1006/abbi.2000.2112

925 42. Hallermalm K, Seki K, Wei C, Castelli C, Rivoltini L, Kiessling R, et al. Tumor necrosis fac-
926 tor-α induces coordinated changes in major histocompatibility class I presentation pathway, re-
927 sulting in increased stability of class I complexes at the cell surface. Blood. 2001;98: 1108–
928 1115. doi:10.1182/blood.v98.4.1108

929 43. Li J, Powell SR, Wang X. Enhancement of proteasome function by PA28α overex-
930 pression protects against oxidative stress. Faseb J Official Publ Fed Am Soc Exp Biology.
931 2010;25: 883–93. doi:10.1096/fj.10-160895

932 44. Fedorova M, Bollineni RC, Hoffmann R. Protein carbonylation as a major hallmark of oxida-
933 tive damage: Update of analytical strategies. Mass Spectrom Rev. 2014;33: 79–97.
934 doi:10.1002/mas.21381

935 45. Dalle-Donne I, Rossi R, Giustarini D, Milzani A, Colombo R. Protein carbonyl groups as bi-
936 omarkers of oxidative stress. Clin Chim Acta. 2003;329: 23–38. doi:10.1016/s0009-
937 8981(03)00003-2

938 46. Ma CP, Willy PJ, Slaughter CA, DeMartino GN. PA28, an activator of the 20 S proteasome,
939 is inactivated by proteolytic modification at its carboxyl terminus. J Biological Chem. 1993;268:
940 22514–9.

941 47. Lesne J, Locard-Paulet M, Parra J, Zivković D, Menneteau T, Bousquet M-P, et al. Confor-
942 mational maps of human 20S proteasomes reveal PA28- and immuno-dependent inter-ring
943 crosstalks. Nat Commun. 2020;11: 6140. doi:10.1038/s41467-020-19934-z

944 48. Xie SC, Metcalfe RD, Hanssen E, Yang T, Gillett DL, Leis AP, et al. The structure of the
945 PA28-20S proteasome complex from Plasmodium falciparum and implications for proteostasis.
946 Nat Microbiol. 2019;4: 1990–2000. doi:10.1038/s41564-019-0524-4

947 49. Nguyen GT, Green ER, Mecsas J. Neutrophils to the ROScue: Mechanisms of NADPH Oxi-
948 dase Activation and Bacterial Resistance. Front Cell Infect Mi. 2017;7: 373.
949 doi:10.3389/fcimb.2017.00373

950 50. Blaser H, Dostert C, Mak TW, Brenner D. TNF and ROS Crosstalk in Inflammation. Trends
951 Cell Biol. 2016;26: 249–261. doi:10.1016/j.tcb.2015.12.002

952 51. Feuvre RAL, Brough D, Iwakura Y, Takeda K, Rothwell NJ. Priming of Macrophages with
953 Lipopolysaccharide Potentiates P2X7-mediated Cell Death via a Caspase-1-dependent Mecha-
954 nism, Independently of Cytokine Production*. J Biol Chem. 2002;277: 3210–3218.
955 doi:10.1074/jbc.m104388200

956 52. Bergsbaken T, Fink SL, Cookson BT. Pyroptosis: host cell death and inflammation. Nat Rev
957 Microbiol. 2009;7: 99 109. doi:10.1038/nrmicro2070

958 53. Qiu J, Luo Z-Q. Hijacking of the Host Ubiquitin Network by Legionella pneumophila. Front
959 Cell Infect Mi. 2017;7: 487. doi:10.3389/fcimb.2017.00487

960 54. Marra A, Blander SJ, Horwitz MA, Shuman HA. Identification of a Legionella pneumophila
961 locus required for intracellular multiplication in human macrophages. Proc National Acad Sci.
962 1992;89: 9607–9611. doi:10.1073/pnas.89.20.9607

963 55. West AP, Brodsky IE, Rahner C, Woo DK, Erdjument-Bromage H, Tempst P, et al. TLR sig-
964 nalling augments macrophage bactericidal activity through mitochondrial ROS. Nature.
965 2011;472: 476 480. doi:10.1038/nature09973

966 56. Fang FC. Antimicrobial reactive oxygen and nitrogen species: concepts and controversies.
967 Nat Rev Microbiol. 2004;2: 820–832. doi:10.1038/nrmicro1004

968 57. Wang X, Chemmama IE, Yu C, Huszagh A, Xu Y, Viner R, et al. The proteasome-interacting
969 Ecm29 protein disassembles the 26S proteasome in response to oxidative stress. J Biol Chem.
970 2017;292: 16310–16320. doi:10.1074/jbc.m117.803619

971 58. Wang X, Yen J, Kaiser P, Huang L. Regulation of the 26S Proteasome Complex During Oxi-
972 dative Stress. Sci Signal. 2010;3: ra88–ra88. doi:10.1126/scisignal.2001232

973 59. Mota-Peynado ADL, Lee SY-C, Pierce BM, Wani P, Singh CR, Roelofs J. The Proteasome-
974 associated Protein Ecm29 Inhibits Proteasomal ATPase Activity and in Vivo Protein Degrada-
975 tion by the Proteasome. J Biol Chem. 2013;288: 29467–29481. doi:10.1074/jbc.m113.491662

976 60. Kiffin R, Bandyopadhyay U, Cuervo AM. Oxidative Stress and Autophagy. Antioxid Redox
977 Sign. 2006;8: 152–162. doi:10.1089/ars.2006.8.152

978 61. Li C, Wang X, Li X, Qiu K, Jiao F, Liu Y, et al. Proteasome Inhibition Activates Autophagy-
979 Lysosome Pathway Associated With TFEB Dephosphorylation and Nuclear Translocation. Fron-
980 tiers Cell Dev Biology. 2019;7: 170. doi:10.3389/fcell.2019.00170

981 62. MacMicking JD. Interferon-inducible effector mechanisms in cell-autonomous immunity. Nat
982 Rev Immunol. 2012;12: 367 382. doi:10.1038/nri3210

983 63. Naujoks J, Tabeling C, Dill BD, Hoffmann C, Brown AS, Kunze M, et al. IFNs Modify the
984 Proteome of Legionella-Containing Vacuoles and Restrict Infection Via IRG1-Derived Itaconic
985 Acid. Zamboni DS, editor. Plos Pathog. 2016;12: e1005408. doi:10.1371/journal.ppat.1005408

986 64. Orvedahl A, McAllaster MR, Sansone A, Dunlap BF, Desai C, Wang Y-T, et al. Autophagy
987 genes in myeloid cells counteract IFNγ-induced TNF-mediated cell death and fatal TNF-induced
988 shock. Proc National Acad Sci. 2019;116: 16497–16506. doi:10.1073/pnas.1822157116

989 65. Byrne BG, Dubuisson J-F, Joshi AD, Persson JJ, Swanson MS. Inflammasome Compo-
990 nents Coordinate Autophagy and Pyroptosis as Macrophage Responses to Infection. Mbio.
991 2013;4: e00620-12. doi:10.1128/mbio.00620-12

992 66. Shin JN, Fattah EA, Bhattacharya A, Ko S, Eissa NT. Inflammasome Activation by Altered
993 Proteostasis*. J Biol Chem. 2013;288: 35886–35895. doi:10.1074/jbc.m113.514919

994 67. Choy A, Dancourt J, Mugo B, O'Connor TJ, Isberg RR, Melia TJ, et al. The Legionella effec-
995 tor RavZ inhibits host autophagy through irreversible Atg8 deconjugation. Science. 2012;338:
996 1072 1076. doi:10.1126/science.1227026

997 68. Rolando M, Escoll P, Nora T, Botti J, Boitez V, Bedia C, et al. Legionella pneumophila S1P-
998 lyase targets host sphingolipid metabolism and restrains autophagy. Proc National Acad Sci.
999 2016;113: 1901 1906. doi:10.1073/pnas.1522067113

1000 69. Rolando M, Escoll P, Buchrieser C. Legionella pneumophila restrains autophagy by modu-
1001 lating the host's sphingolipid metabolism. Autophagy. 2016;12: 1053–1054.
1002 doi:10.1080/15548627.2016.1166325

1003 70. Slater SL, Frankel G. Advances and Challenges in Studying Type III Secretion Effectors of
1004 Attaching and Effacing Pathogens. Front Cell Infect Mi. 2020;10: 337.
1005 doi:10.3389/fcimb.2020.00337

1006 71. Fielden LF, Scott NE, Palmer CS, Khoo CA, Newton HJ, Stojanovski D. Proteomic Identifi-
1007 cation of Coxiella burnetii Effector Proteins Targeted to the Host Cell Mitochondria During Infec-
1008 tion. Mol Cell Proteomics. 2021;20: 100005. doi:10.1074/mcp.ra120.002370

1009 72. Urwyler S, Nyfeler Y, Ragaz C, Lee H, Mueller LN, Aebersold R, et al. Proteome analysis of
1010 Legionella vacuoles purified by magnetic immunoseparation reveals secretory and endosomal
1011 GTPases. Traffic. 2009;10: 76 87. doi:10.1111/j.1600-0854.2008.00851.x

1012 73. Herb M, Schramm M. Functions of ROS in Macrophages and Antimicrobial Immunity. Anti-
1013 oxidants. 2021;10: 313. doi:10.3390/antiox10020313

1014 74. Canton M, Sánchez-Rodríguez R, Spera I, Venegas FC, Favia M, Viola A, et al. Reactive
1015 Oxygen Species in Macrophages: Sources and Targets. Front Immunol. 2021;12: 734229.
1016 doi:10.3389/fimmu.2021.734229

1017 75. Lam GY, Huang J, Brumell JH. The many roles of NOX2 NADPH oxidase-derived ROS in
1018 immunity. Semin Immunopathol. 2010;32: 415–30. doi:10.1007/s00281-010-0221-0

1019 76. Dupré-Crochet S, Erard M, Nüβe O. ROS production in phagocytes: why, when, and where?
1020 J Leukocyte Biol. 2013;94: 657–670. doi:10.1189/jlb.1012544

1021 77. Price CTD, Hanford HE, Vashishta A, Ozanic M, Santic M, Uriarte S, et al. Dot/Icm-Depend-
1022 ent Restriction of Legionella pneumophila within Neutrophils. Mbio. 2021;12: e01008-21.
1023 doi:10.1128/mbio.01008-21

1024 78. Harada T, Miyake M, Imai Y. Evasion of Legionella pneumophila from the Bactericidal Sys-
1025 tem by Reactive Oxygen Species (ROS) in Macrophages. Microbiol Immunol. 2007;51: 1161–
1026 1170. doi:10.1111/j.1348-0421.2007.tb04011.x

1027 79. Gwinn MR, Vallyathan V. Respiratory Burst: Role in Signal Transduction in Alveolar Macro-
1028 phages. J Toxicol Environ Heal Part B. 2007;9: 27–39. doi:10.1080/15287390500196081

1029 80. Forman HJ, Torres M. Reactive Oxygen Species and Cell Signaling. Am J Resp Crit Care.
1030 2002;166: S4–S8. doi:10.1164/rccm.2206007

1031 81. Flynn KJ, Swanson MS. Integrative Conjugative Element ICE-βox Confers Oxidative Stress
1032 Resistance to Legionella pneumophila In Vitro and in Macrophages. Mbio. 2014;5: e01091-14.
1033 doi:10.1128/mbio.01091-14

1034 82. Bandyopadhyay P, Steinman HM. Catalase-Peroxidases of Legionella pneumophila: Clon-
1035 ing of the katA Gene and Studies of KatA Function. J Bacteriol. 2000;182: 6679–6686.
1036 doi:10.1128/jb.182.23.6679-6686.2000

1037 83. Bandyopadhyay P, Byrne B, Chan Y, Swanson MS, Steinman HM. Legionella pneumophila
1038 Catalase-Peroxidases Are Required for Proper Trafficking and Growth in Primary Macrophages.
1039 Infect Immun. 2003;71: 4526–4535. doi:10.1128/iai.71.8.4526-4535.2003

1040 84. Dalle-Donne I, Aldini G, Carini M, Colombo R, Rossi R, Milzani A. Protein carbonylation, cel-
1041 lular dysfunction, and disease progression. J Cell Mol Med. 2006;10: 389–406.
1042 doi:10.1111/j.1582-4934.2006.tb00407.x

1043 85. Dukan S, Farewell A, Ballesteros M, Taddei F, Radman M, Nyström T. Protein oxidation in
1044 response to increased transcriptional or translational errors. Proc National Acad Sci. 2000;97:
1045 5746–5749. doi:10.1073/pnas.100422497

1046 86. Moss SM, Taylor IR, Ruggero D, Gestwicki JE, Shokat KM, Mukherjee S. A Legionella
1047 pneumophila Kinase Phosphorylates the Hsp70 Chaperone Family to Inhibit Eukaryotic Protein
1048 Synthesis. Cell Host Microbe. 2019;25: 454 462.e6. doi:10.1016/j.chom.2019.01.006

1049 87. Rouyère C, Serrano T, Frémont S, Echard A. Oxidation and reduction of actin: Origin, im-
1050 pact in vitro and functional consequences in vivo. Eur J Cell Biol. 2022;101: 151249.
1051 doi:10.1016/j.ejcb.2022.151249

1052 88. Akhter A, Caution K, Abu Khweek A, Tazi M, Abdulrahman BA, Abdelaziz DHA, et al.
1053 Caspase-11 Promotes the Fusion of Phagosomes Harboring Pathogenic Bacteria with Lyso-
1054 somes by Modulating Actin Polymerization. Immunity. 2012;37: 35–47. doi:10.1016/j.im-
1055 muni.2012.05.001

1056 89. Michard C, Sperandio D, Baïlo N, Pizarro-Cerdá J, LeClaire L, Chadeau-Argaud E, et al.
1057 The Legionella Kinase LegK2 Targets the ARP2/3 Complex To Inhibit Actin Nucleation on

1058 Phagosomes and Allow Bacterial Evasion of the Late Endocytic Pathway. Mbio. 2015;6:
1059 e00354-15. doi:10.1128/mbio.00354-15

1060 90. Hervet E, Charpentier X, Vianney A, Lazzaroni J-C, Gilbert C, Atlan D, et al. Protein Kinase
1061 LegK2 Is a Type IV Secretion System Effector Involved in Endoplasmic Reticulum Recruitment
1062 and Intracellular Replication of Legionella pneumophila. Infect Immun. 2011;79: 1936–1950.
1063 doi:10.1128/iai.00805-10

1064 91. Caution K, Gavrilin MA, Tazi M, Kanneganti A, Layman D, Hoque S, et al. Caspase-11 and
1065 caspase-1 differentially modulate actin polymerization via RhoA and Slingshot proteins to pro-
1066 mote bacterial clearance. Sci Rep-uk. 2015;5: 18479. doi:10.1038/srep18479

1067 92. Pignataro M, Rocco GD, Lancellotti L, Bernini F, Subramanian K, Castellini E, et al. Phos-
1068 phorylated cofilin-2 is more prone to oxidative modifications on Cys39 and favors amyloid fibril
1069 formation. Redox Biol. 2020;37: 101691. doi:10.1016/j.redox.2020.101691

1070 93. Seeger M, Ferrell K, Frank R, Dubiel W. HIV-1 Tat Inhibits the 20 S Proteasome and Its 11
1071 S Regulator-mediated Activation*. J Biol Chem. 1997;272: 8145–8148.
1072 doi:10.1074/jbc.272.13.8145

1073 94. Apcher GS, Heink S, Zantopf D, Kloetzel P-M, Schmid H-P, Mayer RJ, et al. Human immu-
1074 nodeficiency virus-1 Tat protein interacts with distinct proteasomal α and β subunits. Febs Lett.
1075 2003;553: 200–204. doi:10.1016/s0014-5793(03)01025-1

1076 95. Stohwasser R, Holzhütter H-G, Lehmann U, Henklein P, Kloetzel P-M. Hepatitis B Virus
1077 HBx Peptide 116–138 and Proteasome Activator PA28 Compete for Binding to the Proteasome
1078 α4/MC6 Subunit. Biol Chem. 2003;384: 39–49. doi:10.1515/bc.2003.005

1079 96. Feeley JC, Gibson RJ, Gorman GW, Langford NC, Rasheed JK, Mackel DC, et al. Char-
1080 coal-yeast extract agar: primary isolation medium for Legionella pneumophila. Journal of clinical
1081 microbiology. 1979;10: 437 441.

1082 97. Saito A, Rolfe RD, Edelstein PH, Finegold SM. Comparison of liquid growth media for Le-
1083 gionella pneumophila. Journal of clinical microbiology. 1981;14: 623 627.

1084 98. Case CL, Roy CR. Analyzing caspase-1 activation during Legionella pneumophila infection
1085 in macrophages. Methods in molecular biology (Clifton, NJ). 2013;954: 479 491.
1086 doi:10.1007/978-1-62703-161-5_29

1087 99. Ingmundson A, Delprato A, Lambright DG, Roy CR. Legionella pneumophila proteins that
1088 regulate Rab1 membrane cycling. Nature. 2007;450: 365–369. doi:10.1038/nature06336

1089 100. Joseph AM, Pohl AE, Ball TJ, Abram TG, Johnson DK, Geisbrecht BV, et al. The Le-
1090 gionella pneumophila metaeffector Lpg2505 (MesI) regulates SidI-mediated translation inhibition
1091 and novel glycosyl hydrolase activity. Infect Immun. 2020;5: e00853-19. doi:10.1128/iai.00853-
1092 19

1093 101. Shames SR, Deng W, Guttman JA, Hoog CL de, Li Y, Hardwidge PR, et al. The patho-
1094 genic E. coli type III effector EspZ interacts with host CD98 and facilitates host cell prosurvival
1095 signalling. Cell Microbiol. 2010;12: 1322 1339. doi:10.1111/j.1462-5822.2010.01470.x

1096 102. Fromont-Racine M, Rain J-C, Legrain P. Toward a functional analysis of the yeast genome
1097 through exhaustive two-hybrid screens. Nat Genet. 1997;16: 277–282. doi:10.1038/ng0797-277

1098 103. Bartel PL, Fields S. [16] Analyzing protein-protein interactions using two-hybrid system.
1099 Methods Enzymol. 1995;254: 241–263. doi:10.1016/0076-6879(95)54018-0

1100 104. Formstecher E, Aresta S, Collura V, Hamburger A, Meil A, Trehin A, et al. Protein interac-
1101 tion mapping: A Drosophila case study. Genome Res. 2005;15: 376–384.
1102 doi:10.1101/gr.2659105

1103

1104

1105 **Figures**

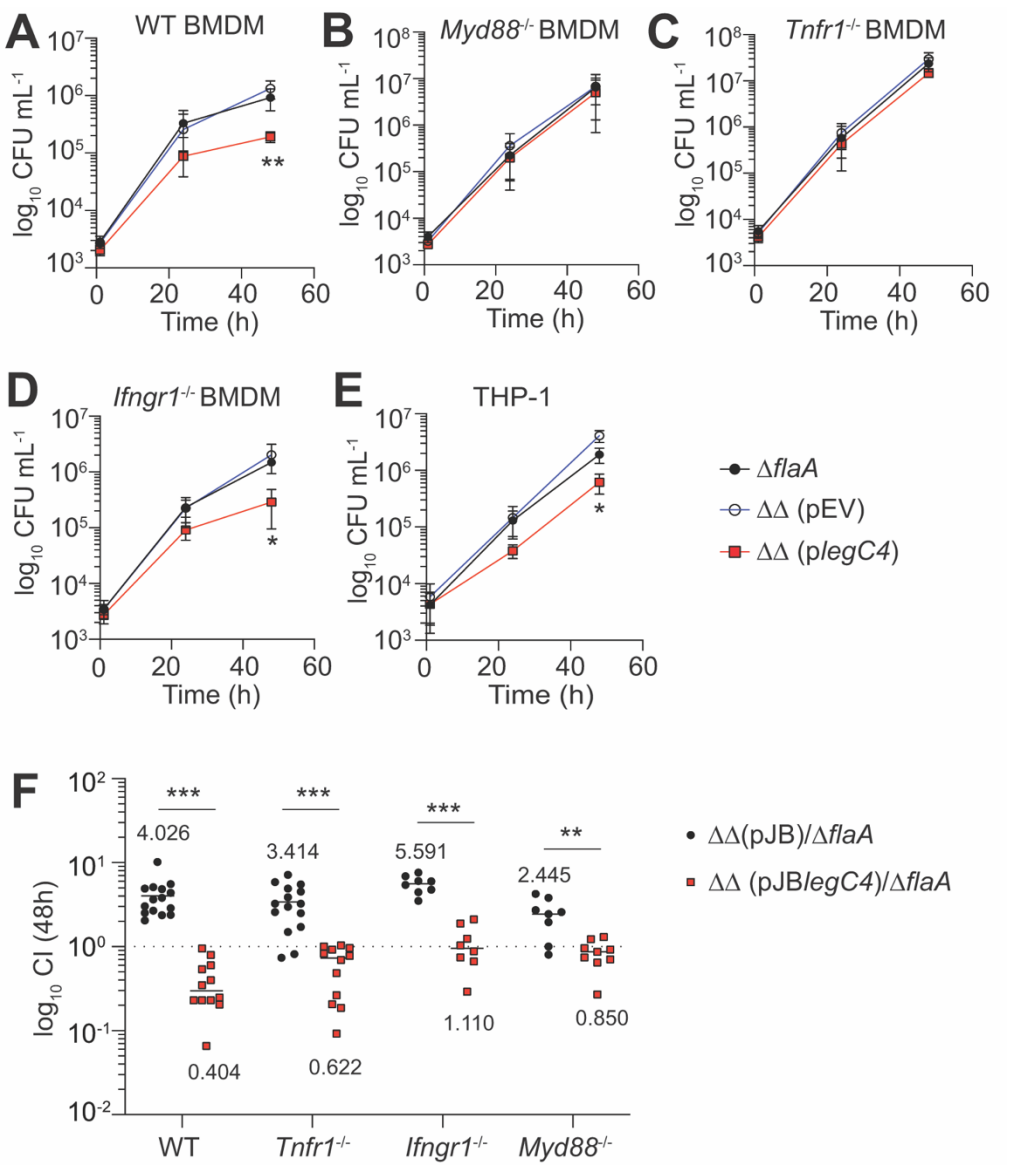

1106

1107 **Figure 1. LegC4 attenuates *L. pneumophila* replication within cytokine-activated macro-**

1108 **phages and the mouse lung.** Growth of indicated *L. pneumophila* strains within **(A)** WT

1109 BMDMs, **(B)** *Myd88*$^{-/-}$ BMDMs, **(C)** *Tnfr1*$^{-/-}$ BMDMs, or **(D)** *Ifngr1*$^{-/-}$ BMDMs, or **(E)** THP-1 cells

1110 over 48 h. Plasmid expression of *legC4* was induced with 1 mM IPTG. Data are shown as mean

1111 ± s.d. of pooled results of at least two independent experiments with triplicate wells per condi-

1112 tion in each experiment. Asterisks denote statistical significance by Students' *t*-test (**P*<0.05,

1113 ***P*<0.01). ΔΔ: Δ*flaA*Δ*legC4*. **(F)** Competitive index (CI) values from the lungs of mice infected

1114 with a 1:1 mixture of *L. pneumophila* ΔΔ (pJB*legC4*) or Δ*flaA*Δ*legC4* (pJB) with *L. pneumophila*

1115 Δ*flaA* at 48 h post-infection. Each symbol represents an individual animal and data are pooled

1116 from at least two independent experiments and mean CI values are shown. Asterisks denote

1117 statistical significance by two-Way ANOVA (***P<0.0001, **P<0.01). ΔΔ: Δ*flaA*Δ*legC4*

1118

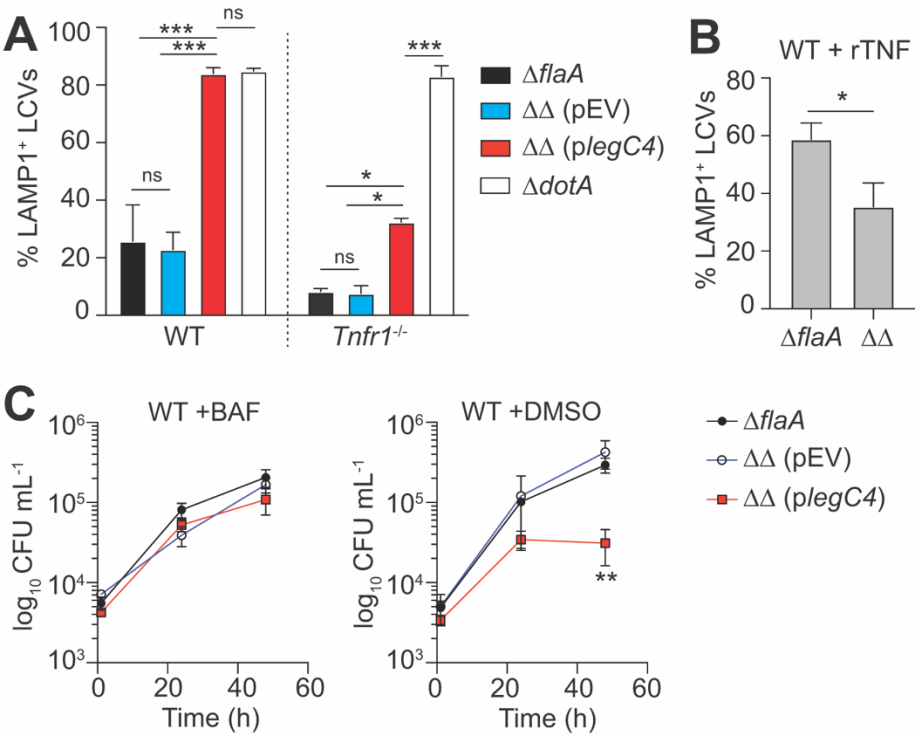

Figure 2. LegC4 enhances phagolysosomal fusion with LCVs and restriction is suppressed by inhibition of the vacuolar (v)ATPase. Abundance of LAMP1+ LCVs within **(A)** naïve WT or *Tnfr1*$^{-/-}$ BMDMs infected with *L. pneumophila* strains for 9h; or **(B)** rTNF-treated WT BMDMs (25 ng mL^{-1}) infected with *L. pneumophila* strains for 6 h. Infections were performed in triplicates and LAMP1 abundance was scored blind (*n*=100 cells per coverslip) by immunofluorescence microscopy (*n*=300 per condition per experiment). Plasmid expression of *legC4* was induced with 1 mM IPTG. Data shown are mean ± s.e.m. of pooled results from two independent experiments (*n*=600 total per condition). Asterisks denote statistical significance by two-way ANOVA (**P*<0.05; ***P*<0.01; ns, not significant). **(C)** Growth of *L. pneumophila* strains within WT BMDMs treated with 10 nM bafilomycin A1 (BAF) (left panel) or DMSO (vehicle control; right panel). Plasmid expression of *legC4* was induced with 1 mM IPTG. Data shown are mean ± s.d. of pooled results from three independent experiments with triplicate samples per experiment. Asterisks denote statistical significance by Students' *t*-test (***P*<0.01). ΔΔ: Δ*flaA*Δ*legC4.*

1134

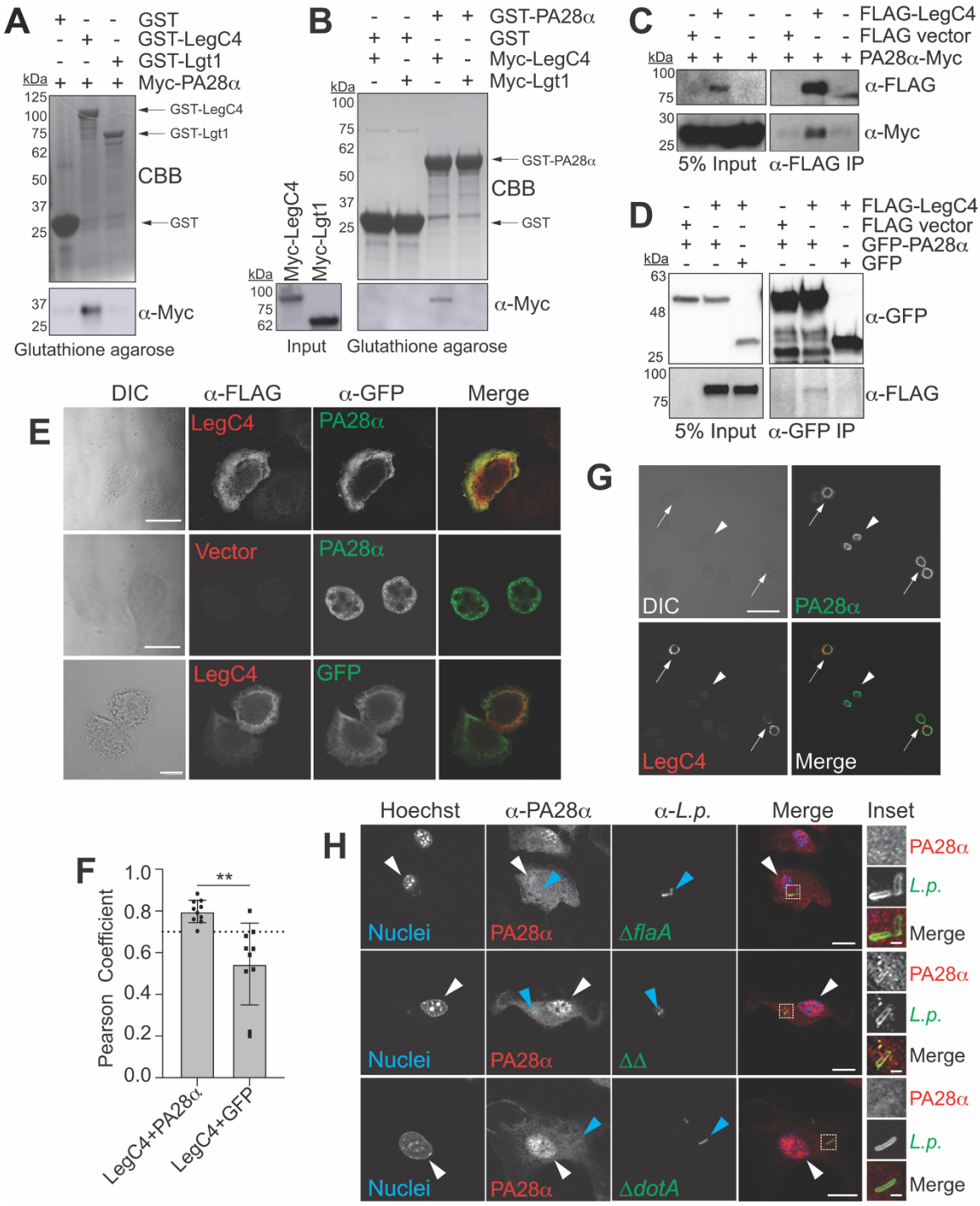

1135

1136 **Figure 3. LegC4 interacts with and alters the subcellular localization of PA28α. (A-B)** Re-

1137 ciprocal affinity chromatography of recombinant GST-fusion proteins from *E. coli* lysates bound

1138 to glutathione agarose beads and incubated with lysates from *E. coli* producing His_6-Myc-fusion

1139 proteins. Proteins retained on the beads were eluted and visualized by SDS-PAGE and Coo-
1140 massie brilliant blue (CBB) stain and α-Myc Western blot. Arrows denote distinct GST-fusion pro-
1141 teins (GST, 26 kDa; GST-LegC4, 113 kDa; GST-Lgt1, 85 kDa; GST-PA28α, 55 kDa; His_6-Myc-
1142 LegC4, 89 kDa; His_6-Myc-Lgt1, 62 kDa; His_6-Myc-PA28α, 31 kDa). Data are representative of
1143 three experiments. **(C)** Western blot of expression (input) and co-immunoprecipitation of PA28α-
1144 Myc with 3xFLAG-LegC4 on a-FLAG conjugated magnetic beads from lysates of co-transfected
1145 HEK293T cells. Data are representative of two independent experiments. (**D**) Western blot of
1146 expression (input) and co-immunoprecipitation of 3xFLAG-LegC4 with GFP-PA28α on α-GFP-
1147 conjugated magnetic beads from lysates of co-transfected HEK 293T cells. Data are representa-
1148 tive of two experiments. **(E)** Representative confocal micrographs of transfected HeLa cells pro-
1149 ducing ectopic 3xFLAG-LegC4 and either GFP-PA28α or GFP stained with α-FLAG and α-GFP
1150 antibodies. Scale bar represents 10 μm. **(F)** Pearson Correlation Coefficients (PCC) were calcu-
1151 lated for individual cells producing 3xFLAG-LegC4 and either GFP-PA28α or GFP alone (n=10)
1152 using Fiji ImageJ software. PCC ≥ 0.7 (dashed line) indicates a high confidence association. As-
1153 terisks denote statistical significance by Students' t-test (**P<0.01). **(G)** Confocal micrograph of
1154 transfected HeLa cells producing GFP-PA28α (arrowhead) or GFP-PA28α and 3xFLAG-LegC4
1155 (arrows). Scale bar represents 50 μm. **(H)** Confocal micrographs of WT BMDMs infected with *L.*
1156 *pneumophila* strains (MOI of 25) for 7h and stained with α-PA28α (red) and α-*L. pneumophila*
1157 (green) antibodies. Cellular nuclei were imaged with Hoechst (blue). White and blue arrowheads
1158 indicate BMDM nuclei and intracellular bacteria, respectively. Scale bar represents 10 μm. Inset
1159 images are magnified from regions indicated with white boxes. Scale bar represents 1 μm. Images
1160 are representative of populations of infected BMDMs over two independent experiments. ΔΔ:
1161 Δ*flaA*Δ*legC4*
1162
1163

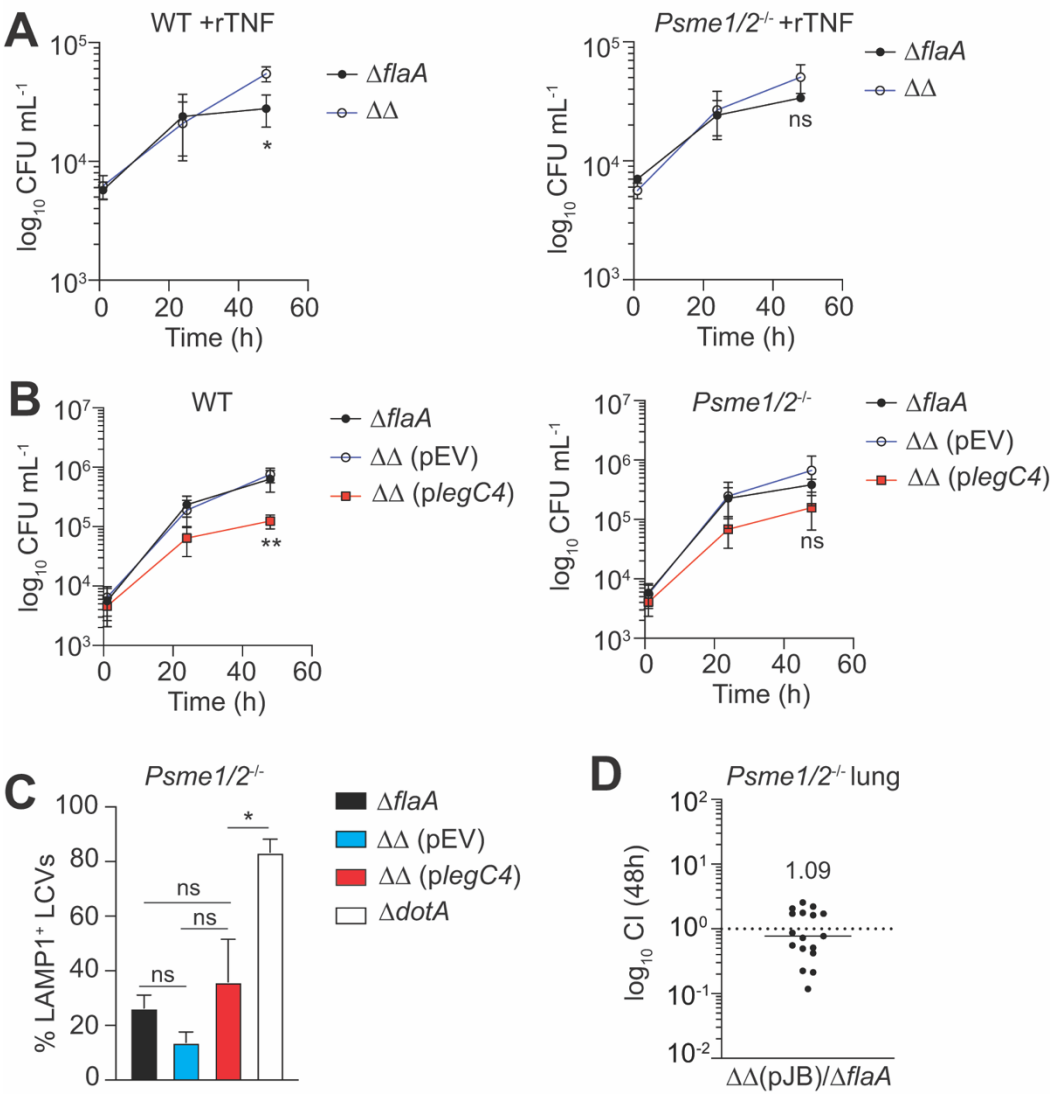

1164

1165 **Figure 4**. **PA28αβ is important for LegC4 restriction phenotypes within cultured BMDMs**
1166 **and the mouse lung *in vivo*.** Growth of *L. pneumophila* strains within rTNF-treated **(A)** or naïve
1167 **(B)** WT (top) or *Psme1/2*$^{-/-}$ (bottom) BMDMs. Where indicated, BMDMs were treated with 25 ng
1168 mL^{-1} rTNF and plasmid expression of *legC4* was induced with 1 mM IPTG. Data shown are mean
1169 ± s.d. of pooled results from three independent experiments with triplicate samples per condition
1170 in each experiment. Asterisks denote statistical significance by Students' *t*-test (***P*<0.01;
1171 **P*<0.05). ns, not significant. **(C)** Quantification of LAMP1^{+} LCVs within *Psme1/2*$^{-/-}$ BMDMs in-
1172 fected with *L. pneumophila* strains for 9h. Infections were performed in triplicates and LAMP1^{+}
1173 LCVs were scored blind (*n*=50 infected cells per coverslip) by immunofluorescence microscopy

1174 (*n*=150 per condition per experiment). Data shown are mean ± s.e.m. of pooled results of three
1175 independent experiments (*n*=450 total per condition) and asterisks denote statistical significance
1176 by two-way ANOVA (**P*<0.05). ns, not significant. Plasmid expression of *legC4* was induced with
1177 1 mM IPTG. **(D)** Competitive index (CI) values from the lungs of *Psme1/2*$^{-/-}$ mice infected with a
1178 1:1 mixture of *L. pneumophila* ΔΔ (pJB) and *L. pneumophila* Δ*flaA* at 48 h. Each symbol repre-
1179 sents an individual animal and data are pooled from three independent experiments. The mean
1180 CI value is shown. ΔΔ: Δ*flaA*Δ*legC4.*
1181

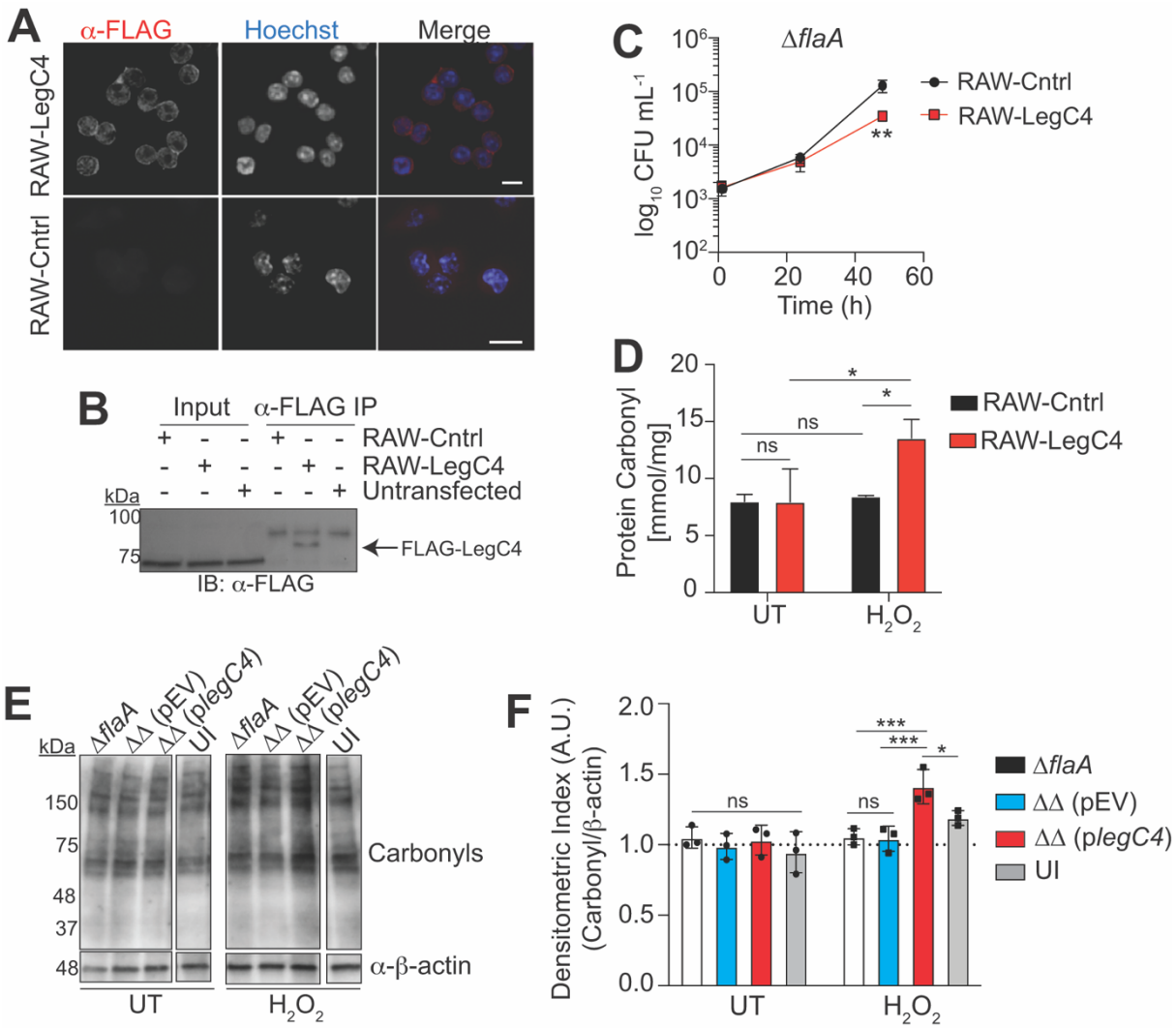

Figure 5. The abundance of carbonylated proteins is increased in the presence of LegC4 under oxidative stress conditions. **(A)** Representative confocal micrographs of RAW-LegC4 and -Cntrl cells stained with α-FLAG antibodies and Hoechst to image nuclei. Scale bar represents 10 μm. **(B)** Western blot of α-FLAG immunoprecipitation from lysates of RAW-LegC4, RAW-Cntrl or untransfected (UT) RAW cells with α-FLAG primary antibody. Arrow indicates 3xFLAG-LegC4 (~84 kDa). **(C)** Growth of *L. pneumophila* Δ*flaA* within RAW-LegC4 and -Cntrl cells. Data shown are mean ± s.d. of pooled results of three independent experiments with triplicate samples per condition in each experiment. Asterisks denote statistical significance by Students' *t*-test (**P<0.01). **(D)** Quantification of protein carbonyls by ELISA in lysates of RAW-LegC4 and -Cntrl

1192 cells incubated in low-serum media for 24 h in the presence or absence of 10 μM H_2O_2. Data
1193 shown are mean ± s.e.m. and representative of two independent experiments. Asterisks denote
1194 statistical significance by two-way ANOVA (*P<0.05; ns, not significant). UT: untreated. **(E)** West-
1195 ern blot for protein carbonyls and β-actin (loading control) in lysates of *Tnfr1*$^{-/-}$ BMDMs infected
1196 for 4 h with the indicated strains (MOI of 50) in the presence or absence of 50 μM H_2O_2. Uninfected
1197 (UI) samples are from the same experiment but shown separately to remove irrelevant lanes. ΔΔ:
1198 Δ*flaA*Δ*legC4*; plasmid expression of *legC4* was induced with 1 mM IPTG. Data are representative
1199 of three independent experiments. **(F)** Densitometric quantification of carbonylated proteins from
1200 Western blots. Signal intensity from protein carbonyl Western blots was normalized to the β-actin
1201 loading control for each sample and averaged ratios were normalized to Δ*flaA*-infected cells. Data
1202 shown are mean ± s.d. of values from three independent experiments. Asterisks denote statistical
1203 significance by two-way ANOVA (**P<0.01; *P<0.05). ns, not significant.
1204

1205

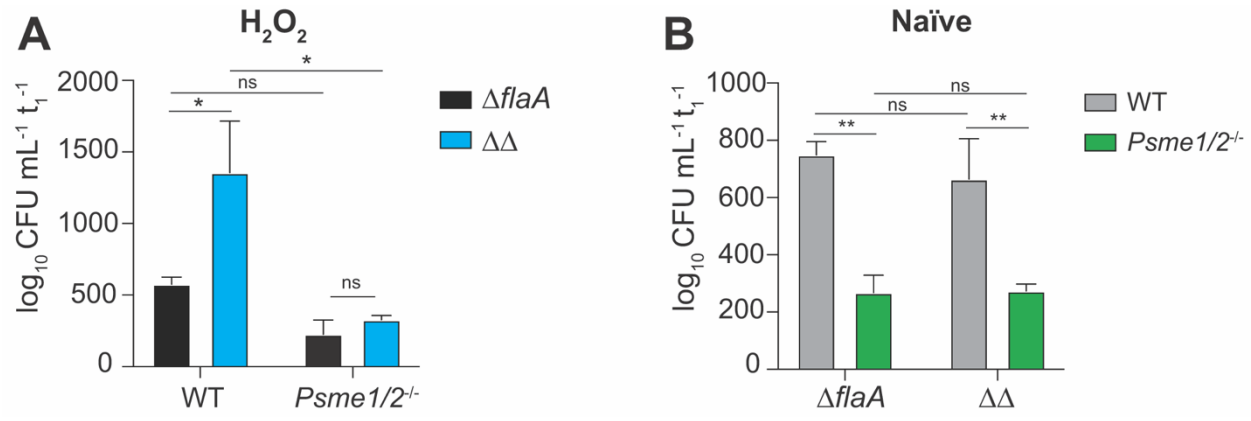

1206

1207 **Figure 6. LegC4 restriction occurs under oxidative stress conditions and is phenocopied**

1208 **by loss of PA28αβ.** Normalized CFU recovered from **(A)** 20 μM H_2O_2-treated or **(B)** naïve WT

1209 or *Psme1/2*$^{-/-}$ BMDMs infected for 48 h with either *L. pneumophila* Δ*flaA* or ΔΔ. CFU of each

1210 strain recovered at 48 h was normalized to internalized bacteria at 1h post-infection for each

1211 condition. Data shown are mean ± s.e.m. of pooled results from three independent experiments

1212 with triplicate samples per condition in each experiment. Asterisks denote statistical significance

1213 by two-way ANOVA (**P<0.01, *P<0.05). ns, not significant.

1214

1215